Uncertainty Analysis of an Aviation Climate Model and an Aircraft Price Model for Assessment of Environmental Effects

by

Mina Jun

Submitted to the Department of Aeronautics and Astronautics
in partial fulfillment of the requirements for the degree of

Master of Science in Aeronautics and Astronautics

at the

MASSACHUSETTS INSTITUTE OF TECHNOLOGY

September 2007

Author .....
Department of Aeronautics and Astronautics
August 23, 2007

Certified by .....
Ian Waitz
Jerome C. Hunsaker Professor of Aeronautics and Astronautics
Thesis Supervisor

Accepted by .....
David L. Darmofal
Associate Professor of Aeronautics and Astronautics
Chair, Committee on Graduate Students

Uncertainty Analysis of an Aviation Climate Model and an Aircraft Price Model for Assessment of Environmental Effects

by

Mina Jun

Submitted to the Department of Aeronautics and Astronautics
on August 23, 2007, in partial fulfillment of the
requirements for the degree of
Master of Science in Aeronautics and Astronautics

Abstract

Estimating, presenting, and assessing uncertainties are important parts in assessment of a complex system.

This thesis focuses on the assessment of uncertainty in the price module and the climate module in the Aviation Environmental Portfolio Management Tool (APMT). The aircraft price module is a part of the Partial Equilibrium Block (PEB) and the climate module is a part of the Benefits Valuation Block (BVB) of the APMT. The PEB estimates a future fleet and flight schedule and evaluates manufacturer costs, operator costs, and consumer surplus. The BVB estimates changes in health and welfare for climate, local air quality, and noise from noise and emissions inventories output from the Aviation Environmental Design Tool (AEDT).

The assessment was conducted with various uncertainty assessment and sensitivity analysis methods: the nominal range sensitivity analysis (NRSA), the hybrid Monte Carlo sensitivity analysis, the Monte Carlo regression analysis, the vary-all-but-one Monte Carlo analysis, and the global sensitivity analysis with Sobol' indices and total sensitivity indices. Except the NRSA, all other analysis methods are based on the Monte Carlo simulation with random sampling.

All uncertainty assessment methods provided the same ranking of significant variables in both APMT modules. Two or three significant variables are clearly distinguished from other insignificant variables. In the price module, seat coefficients are the most significant parameters, and age is an insignificant factor between input variables of the regression model. In the climate module, statistical analyses showed that climate sensitivity and short-lived RF are most significant variables that contribute the variability of all three outputs. However, the HMC analysis suggested that discount rate is the most sensitive factor in the NPV estimation. Comparing the Sobol's indices with the total sensitivity indices showed that there are no significant interactions to change the ranking of significant variables in both modules.

Thesis Supervisor: Ian Waitz
Title: Jerome C. Hunsaker Professor of Aeronautics and Astronautics

Acknowledgments

I would like to thank my advisor, Prof. Ian Waitz, deeply. I was able to make the first step as a researcher with opportunities he gave me, and to complete this thesis with his insightful advice and endless support. I also appreciate his patience and belief in my work. I also thank Prof. Karen Willcox for her advice and useful expertise.

I wish to express special thanks to Karen Marais and Anuja Mahashabde who have worked with me in the climate model. They were the best colleagues and the best friends at the same time. Next, I want to thank all APMT team members. It was my pleasure to work with such brilliant people.

I thank my parents, my grandmother, and my sister and brother. They always give me enormous love and encouragement.

Jun-geun, I want to tell him how much I love him. He is my best supporter and the best friend who understands me deeply. I also thank my little friends. They please me and give a smile everyday.

This work was supported by the Korea Science and Engineering Foundation Grant funded by the Korea government (No.D00076) and also by the U.S. Federal Aviation Administration, Office of Environment and Energy, under the contract number DTWF A-05-D-00012, Task Order No. 0002 and managed by Maryalice Locke.

Contents

List of Figures

List of Tables

Chapter 1

Introduction

1.1 Background

Uncertainty and sensitivity analysis is an important part of assessing a complex model. There are two types of uncertainty [19, 26]. The first is stochastic uncertainty which comes from variability of the system itself. The second is subjective uncertainty which comes from insufficient knowledge of the correct value of system parameters or inputs. Both stochastic and subjective uncertainties are investigated in this thesis with two different models, an aircraft price model and a climate model. The uncertainty relative to the price model is stochastic uncertainty, and the uncertainty in input variables of the climate model, except emissions scenarios and discount rate, is an example of subjective uncertainty.

The aircraft price model and the climate model are components of a larger analysis tool, the Aviation Environmental Portfolio Management Tool (APMT), being developed by the U.S. Federal Aviation Adminstration Office of Environment and Energy (FAA-AEE). The goal of APMT is to assess the environmental and economic impacts of different potential policies. There are five different functional blocks: the Partial Equilibrium Block, the Aviation Environmental Design Space Block, the Benefits Valuation Block, the General Economy Block, and the Analysis and Display Block [11]. The aircraft price module is a part of the Partial Equilibrium Block (PEB) and the climate module is a part of the Benefits Valuation Block (BVB). The PEB estimates a future fleet and flight schedule and evaluates manufacturer costs, operator costs, and consumer surplus. The PEB can take future technology aircraft from the Environmental Design Space (EDS) which estimates source noise, exhaust emissions, performance, and economic parameters for aircraft designs.

Manufacturer cost and aircraft price are based on a price regression model of historical data. The regression model to estimate aircraft price relates aircraft price and performance characteristics of aircraft. The BVB estimates changes in health and welfare for climate, local air quality, and noise from noise and emissions inventories output from the Aviation Environmental Design Tool (AEDT). Benefit-cost analysis can be performed with the cost evaluated from changes in health and welfare. The climate module estimates the surface temperature change and associated costs from fuel burn, CO_2, and NO_x inventories based on impulse response functions derived from climate models.

1.2 Previous Work

Uncertainty assessment and sensitivity analysis techniques have been studied and applied to various systems. Helton [19] summarized and compared different approaches to uncertainty and sensitivity analyses and implemented those in the assessment of the Waste Isolation Pilot. This study focused on the analysis of subjective uncertainty. Another example of the implementation of uncertainty assessment methods is the study of Ma et al. [3], where both local and global sensitivity analyses were conducted for the parameter analysis of hysteresis models. Sobol index and total effect index were adopted for the global sensitivity analysis to analyze significant parameters and their interactions. For variance based global sensitivity analyses, the Fourier amplitude sensitivity test (FAST) was introduced in 1970s [7, 41, 8, 8] and the Sobol' sensitivity indices were presented in 1990 [43]. Although FAST is more robust and faster than Sobol' indices, Sobol's indices have a more general form to evaluate high order interaction terms and the total effect [38]. There are also various techniques for the uncertainty assessment, such as Design of Experiments, Response Surface methods, and Monte Carlo simulation, as well as variance based methods [30].

Many uncertainty studies about the climate change have been conducted for both physical uncertainty and economic uncertainty. Hulme and Carter [23] summarized the different types of uncertainties expected in the climate change scenarios and compared different methods for estimating, describing, and comparing uncertainties. New and Hulme assessed the uncertainty relative to climate change impacts by using a Monte Carlo approach. The study quantified the uncertainty in different emissions scenarios, climate sensitivity, and the general circulation model (GCM) [33]. As well as assessing physical impacts, Newell

and Pizer studied the impacts of discount rate in the climate policy [35], and Tol studied the uncertainties of climate change relative to the cost-benefit analysis in terms of CO_2 emissions costs [47]. The studies showed that the economic uncertainty in climate change is significant when considering the impacts long into the future.

This thesis will introduce and compare various uncertainty assessment and sensitivity analysis techniques including local and global sensitivity analyses and deterministic and variance based methods. Also, those analysis methods will be implemented in the assessment of uncertainty in the price module of the PEB and the climate module of the BVB in the APMT tool, where uncertainty will be assessed for outputs of both physical and economic metrics in the climate module.

1.3 Thesis Objectives and Contributions

This thesis aims to understand the different types of uncertainty analysis and analyze the uncertainty in two different modules of the APMT tool. When investigating how uncertainties are propagated through to system level metrics, assessing uncertainty propagation through an individual module will be a basis of entire system level assessment because modules composing a system are linked through common inputs or outputs. This thesis will assess how different uncertainty analysis methods affect the analysis result and evaluate the methods.

The main contributions of this thesis are:

- Major uncertainty sources in the price module and the climate module are identified.
- Implementation of uncertainty analysis methods are described in detail. This includes how to define input distributions and how to check the convergence error.
- Different types of uncertainty analyses like local or global sensitivity analysis and deterministic or probabilistic sensitivity analysis are compared.
- A general scheme for uncertainty assessment is suggested.

Chapter 2

Uncertainty and Sensitivity Analysis Method

This chapter introduces uncertainty assessment methods used in this thesis. There are two classes of sensitivity analysis, statistical methods and deterministic methods. Statistical methods are based on sampling from probabilistic distributions and analyze the variance of outputs, while deterministic methods are used for analyzing the local system response to perturbations. Also, sensitivity analysis can be classified according to its scope, local analysis and global analysis. A local sensitivity is focused on the system response around a selected point, and a global sensitivity analyzes the characteristics of the system in the entire modeling space. Although both statistical and deterministic methods can be applicable at the local and global scope, deterministic methods normally use local sensitivity indices and statistical methods use both local and global sensitivity indices [4]. The following section describes the basic ideas and the approaches to capture the impacts of parameters to the output variability. The methods to be presented include the Monte Carlo analysis, the vary-all-but-one Monte Carlo analysis, and the global sensitivity analysis as statistical methods, and the nominal range sensitivity analysis as a deterministic analysis. Most assessment efforts are focused on the statistical methods with sampling to address the impacts of uncertainty in the possible range of input variables. The contribution of variables to the output variability can be explained with two effects: a main effect and an interaction effect. A main effect is the effect of a factor alone on an output variable, which is only affected by levels of the considered variable. An interaction effect is the effect of one more factors

which influence each other; that is, the effect of one variable on an output depends on the specific values of other variables. According to the statistical type of assessment methods, sensitivity indices capture both of or each of these effects. Therefore, according to what kinds of effects can be expected and how a system is modeled, different types of methods can be applied to assessment.

2.1 Nominal Range Sensitivity Analysis

The nominal range sensitivity analysis (NRSA) [12] is a local sensitivity analysis method. It is straightforward to compute sensitivity indices of the NRSA as shown in Equation 2.1.

$$\text{sensitivity}_{x_j} = \frac{f(x_{1_n}, \cdots, x_{j_u}, \cdots, x_{n_n}) - f(x_{1_n}, \cdots, x_{j_l}, \cdots, x_{n_n})}{f(\mathbf{x}_n)} \tag{2.1}$$

where $\mathbf{x} = [x_1, x_2, \cdots, x_n]$ and subscript n means a nominal value, l means a value of lower range, and u means a value of upper range. The impact of an input variable or a parameter is easily calculated without expensive computing power by varying it at a time, but it cannot investigate the probabilistic uncertainty and interactions between variables. Also, if a model is nonlinear, the result of the analysis would be very different according to the variable range that is considered. While the NRSA is best suited for a deterministic model, it is extensible to incorporate Monte Carlo (MC) simulation for a probabilistic model. This composite method is called the hybrid Monte Carlo (HMC) sensitivity analysis in this thesis. In the hybrid Monte Carlo sensitivity analysis, some of input variables and parameters are varied between upper and lower ranges deterministically like the NRSA, but other input variables and parameters are drawn from a probabilistic distribution like Monte Carlo simulation, as shown in Equation 2.2. Deterministic variables can be chosen based on the analysis interest. For example, the hybrid Monte Carlo analysis can investigate the impacts of key uncertain variables at the limits of their nominal ranges by choosing those key variables as deterministic variables. The result is more comprehensive than the NRSA result because it includes the interaction effects of probabilistic variables. Therefore, the hybrid Monte Carlo analysis can provide better sensitivity information if probabilistic modeling is needed or the best estimates for variables are not available.

$$\text{HMC sensitivity}_{x_j} = \frac{f(x_{\mathbf{f}_{1n}}, \cdots, x_{\mathbf{f}_{j_u}}, \cdots, x_{\mathbf{f}_{k_n}}, \mathbf{x_d}) - f(x_{\mathbf{f}_{1n}}, \cdots, x_{\mathbf{f}_{j_l}}, \cdots, x_{\mathbf{f}_{k_n}}, \mathbf{x_d})}{f(\mathbf{x}_{\mathbf{f}n}, \mathbf{x_d})} \tag{2.2}$$

where

$$\mathbf{x} = [\mathbf{x_f}, \mathbf{x}_d]$$

$\mathbf{x_f}$ is deterministic, $\mathbf{x_f} = [x_1, \cdots, x_k]$ $k \leq n$

$\mathbf{x_d}$ is randomly sampled, $\mathbf{x_d} = [x_{k+1}, \cdots, x_n]$

2.2 Monte Carlo Analysis

Monte Carlo analysis is a common method to investigate the uncertainty inside a model or how key input variables contribute to the uncertainty of outputs. The method randomly draws samples of input variables from defined probabilistic distributions and propagate the uncertainty in inputs through a model. As a result, Monte Carlo analysis can assess uncertainty with numerical output results and input samples without any analytical form of outputs and inputs. It is generally illustrated with five steps [19].

First, input variables are represented statistically. This step relates the uncertainty of variables to probabilistic distributions. Although accurate distributions for input variables are desired in this step to obtain precise information about the output distribution, usually it is enough to assume input variables can be represented by simple distributions, such as uniform or triangular, when assessing their contributions to the output uncertainty. Second, values for input variables are sampled from defined distributions. One of basic sampling methods is pseudo-random sampling. The pseudo-random Monte Carlo method is called commonly the Monte Carlo method. Stratified sampling is used to ensure more uniform sampling through the design space than pseudo-random sampling. It divides the design space into several sub-regions and generates random samples in each sub-region. Modern sampling techniques include Latin hypercube sampling and orthogonal array sampling. These methods estimate output statistics more accurately if sampling size is identical to that of the basic random sampling method. Giuta et al. provided an overview of these sampling methods and algorithms as well as a comparison of methods [14]. Third, the uncertainty is propagated through a simulation model. A model generates a sequence of a output variable(s) from samples of input variables, as shown in Equation 2.3.

$$y_i = f(x_{i1}, x_{i2}, \cdots, x_{im}) = f(\mathbf{x_i}), \quad i = 1, 2, \cdots, m \tag{2.3}$$

Forth, uncertainty analysis is conducted with the simulation result. A simple way to present the uncertainty of outputs is to estimate the mean and variance of outputs. A distribution function or box plots provides more information regarding the output distributions such as cumulative probability or quantiles as well as graphical presentation of results. Finally, sensitivity analysis is conducted to investigate the relationship between inputs and outputs. Regression analysis based on Equation 2.4 can provide good screening information for determining important input variables. The least squares method is commonly used to estimate the coefficients, β_j.

$$y = \beta_0 + \sum_{j=1}^{n} \beta_j x_j \tag{2.4}$$

The regression model in Equation 2.4 can be transformed to the standardized form in Equation 2.5. [27]

$$y^* = \sum_{j=1}^{n} \beta_j^* x_j^* \tag{2.5}$$

where

$$y^* = \frac{1}{\sqrt{m-1}} \left(\frac{y - \bar{y}}{s_Y} \right), \quad \bar{y} = \frac{1}{m} \sum_{i=1}^{m} y_i$$

$$x_j^* = \frac{1}{\sqrt{m-1}} \left(\frac{x_j - \bar{x}_j}{s_j} \right), \quad \bar{x}_j = \frac{1}{m} \sum_{i=1}^{m} x_{ij}$$

$$s_Y = \sqrt{\frac{\sum_{i=1}^{m} (y_i - \bar{y})^2}{m-1}}$$

$$s_k = \sqrt{\frac{\sum_{i=1}^{m} (x_{ij} - \bar{x}_j)^2}{m-1}}$$

The standardized regression coefficients, β_j^*, are related to the original regression coefficients, β_j, by a scaling factor in Equation 2.6.

$$\beta_j^* = \left(\frac{s_k}{s_Y} \right) \beta_j \tag{2.6}$$

Since different units of x_i and x_j are normalized in the standardized regression coefficients, β_j^* can be a direct indicator of the impact of input variables to the mean shift of outputs. Also, a t-test can be conducted to test the significance of the coefficients.

Regression analysis based on Monte Carlo simulations is efficient especially when there

are many input variables because the analysis can be conducted with only one Monte Carlo simulation independent of the number of input variables. In contrast, other sensitivity analyses require a series of Monte Carlo simulations of at least the number of input variables. If the model includes significant interactions between input variables or is nonlinear, however, the first order linear regression analysis would result in inaccurate assessment of contributions between variables. Adding higher order terms can be a solution, but there is a possibility of overfitting which results in a poor estimation of results. Comparing mean squared prediction error (MSPR) of the predicted error sum of squares (PRESS) and the mean squared error (MSE) of the regression model or MSPR of other regression models can indicate the overfitting problem. The PRESS of Equation 2.8 is a similar form to the sum of squared error (SSE) of Equation 2.7 but it is the sum of predicted errors omitting the ith observation to obtain the fitted value, $\hat{Y}_i$. That is, the regression model is based on the (m-1) observations, which are the subset of the full data set, and the output value for the ith observation is predicted from the regression model based on (m-1) observations. The notation $Y_{i(i)}$ is used for the predicted value of ith observation indicated by the first i when ith observation, the second i in parentheses, is omitted.

$$\text{SSE} = \sum_{i=1}^{m}(Y_i - \hat{Y}_i)^2 \tag{2.7}$$

where $\hat{Y}_i$ is a fitted value

$$\text{PRESS}_p = \sum_{i=1}^{m}(Y_i - \hat{Y}_{i(i)})^2 \tag{2.8}$$

Comparing the PRESS value and choosing the regression model with the smallest PRESS value is a good strategy for choosing a better but not overfitted regression model because small PRESS values indicate a good prediction power of the regression model. Or, if PRESS MSPR, PRESS/(m-1), is close to the MSE of the regression model based on the full data set, the model can be regarded as not overfitted because the close consistency of PRESS MSPR and MSE means that MSE is a good indicator of the model predictive ability [27].

Using a series of Monte Carlo simulations, it is possible to assess the uncertainty of a model with more precise sensitivity analysis. Two techniques, the vary-all-but-one Monte Carlo analysis and the global sensitivity analysis are introduced in the following sections.

Although additional Monte Carlo simulation runs are required as many as the number of input variables, these method do not assume an approximated model to estimate sensitivity indices.

2.3 Vary-all-but-one Monte Carlo Analysis

Vary-all-but-one (VABO) Monte Carlo simulation uses a series of Monte Carlo simulations where the uncertainty of one parameter is removed at a time [28]. VABO Monte Carlo analysis requires a total $n + 1$ Monte Carlo simulations, where n is the number of input variables. One more Monte Carlo simulation with all varying input variables is need for a baseline in addition to n Monte Carlo simulations. The jth input variable is fixed at a base value, c_{ij}, and other input variables, $x_i (i \neq j)$, are drawn from defined distributions for the vary-all-but-jth variable Monte Carlo simulation, as shown in Equation 2.9.

$$y_{i,j_F} = f(x_{i1}, x_{i2}, \cdots, x_{i(j-1)}, c_{ij}, x_{i(j+1)}, \cdots, x_{in}), \quad i = 1, 2, \cdots, m \tag{2.9}$$

This method allows the investigation of a parameter's contribution to mean and variance shifts in Equation 2.10 without any assumption about underlying distribution shape or linearity. However, it requires a good choice or understanding of base values because different results can be drawn according to the choice of values if the model has non-linearity.

$$\begin{aligned} \text{mean shift caused by } x_j &= \frac{\bar{y} - \bar{y}_{j_F}}{\bar{y}} \\ \text{variance shift caused by } x_j &= \frac{\sigma^2 - \sigma^2_{j_F}}{\sigma^2} \end{aligned} \tag{2.10}$$

where $$\bar{y}_{j_F} = \frac{1}{m}\sum_{i=1}^{m} y_{i,j_F}, \quad \sigma^2_{j_F} = \frac{1}{m-1}\sum_{i=1}^{m}(y_{i,j_F} - \bar{y}_{j_F})^2$$

2.4 Global Sensitivity Analysis

The local sensitivity analysis or the VABO Monte Carlo analysis provide sensitivity indices of input variables near interesting points. In contrast, the global sensitivity analysis provides sensitivity indices of input variables over the entire ranges rather at a point. The basic concept of global sensitivity analysis is a measure of variance apportionment. M.

Sobol' proposed general global sensitivity indices based on an ANOVA-representation of an integrable function $f(x)$ in the form of Equation 2.11 [45].

$$\begin{aligned} f(x) &= f_0 + \sum_{s=1}^{n} \sum_{j_1<\cdots<j_s}^{n} f_{j_1\cdots j_s}(x_{j_1}, \ldots, x_{j_s}) \\ &= f_0 + \sum_{j=1}^{n} f_j(x_j) + \sum_{j<k} f_{jk}(x_j, x_k) + \cdots + f_{12\cdots n}(x_1, x_2, \cdots, x_n) \end{aligned} \tag{2.11}$$

Equation 2.11 is called an ANOVA-representation of $f(x)$ if Equation 2.12 is satisfied.

$$\int_0^1 f_{j_1\cdots j_s}(x_{j_1}, \cdots, x_{j_s}) dx_k = 0 \text{ for } k = i_1, \ldots, i_s \tag{2.12}$$

These definitions lead to the orthogonality of components in Equation 2.11 as shown in Equation 2.13.

$$\int f_{j_1\cdots j_s} \cdot f_{k_1\cdots k_t} d\mathbf{x} = 0 \tag{2.13}$$

As a result, the components in Equation 2.11 can be calculated as integrals like Equation 2.14–2.16 and so on.

$$\int f(\mathbf{x}) d\mathbf{x} = f_0 \tag{2.14}$$

$$\int f(\mathbf{x}) d\mathbf{x}_{\sim j} = f_0 + f_j(x_j) \tag{2.15}$$

$$\int f(\mathbf{x}) d\mathbf{x}_{\sim j,k} = f_0 + f_j(x_j) + f_k(x_k) + f_{jk}(x_j, x_k) \tag{2.16}$$

where $\mathbf{x}_{\sim j}$ means all input variables except x_j. With this integral expression,the global sensitivity indices are introduced as the ratio in Equation 2.17.

$$S_{j_1\cdots j_s} = \frac{D_{j_1\cdots j_s}}{D} \tag{2.17}$$

where

$$D = \int f^2 d\mathbf{x} - f_0^2$$

$$D_{j_1\cdots j_s} = \int \cdots \int f^2_{j_1\cdots j_s} dx_{j_1} \cdots dx_{j_s}$$

D indicate the total variance of $f(x)$, and $D_{j_1 \cdots j_s}$ is the variance of $f^2_{j_1 \cdots j_s}(x_{j_1}, \cdots, x_{j_s})$. From Equation 2.17 and 2.13, all global sensitivity indices are positive and

$$\sum_{s=1}^{n} \sum_{j_1 < \cdots < j_s}^{n} S_{j_1 \cdots j_s} = 1 \tag{2.18}$$

To evaluate all global sensitivity indices, 2^n sampling and $m \times 2^n$ computation is required. If input variables are many, calculation of all sensitivity indices for interactions requires extensive computation effort. Since the sum of a main effect of the parameter and all high order interaction effects related to the parameter is meaningful rather than each individual effect when evaluating the effect of input variables to variation of output, Homma and Saltelli suggested a new sensitivity index, total sensitivity, for the sum of all effects related to one parameter, which are directly calculated from n samples rather than calculated from individual effect [21]. Total variance can be decomposed with the variance from x_j, the variance from the interaction of x_j and all other input variables, and the variance from all other input variables and their interactions. That is,

$$D = D_j + D_{j,\sim j} + D_{\sim j} \tag{2.19}$$

Divided by the total variance, Equation 2.19 is represented in terms of global sensitivity indices.

$$1 = S_j + S_{j,\sim j} + S_{\sim j} \tag{2.20}$$

Total sensitivity of the jth variable is defined as the sum of a x_j main effect and interaction effects related to x_j, as shown in Equation 2.21

$$S_{T_j} = S_j + S_{j,\sim j} = 1 - S_{\sim j} \tag{2.21}$$

Therefore, the total sensitivity can be calculated from $S_{\sim j}$ instead of all $S_{j,\sim j}$'s.

2.4.1 Monte Carlo Computation

Integrals for the global sensitivity can be estimated with the following Monte Carlo integrals.

$$\hat{f}_0 = \frac{1}{m} \sum_{i=1}^{m} f(\mathbf{x_i}) \tag{2.22}$$

$$\hat{D} = \frac{1}{m}\sum_{i=1}^{m} f(\mathbf{x_i})^2 - \hat{f}_0^2 \tag{2.23}$$

$$\hat{D}_j = \frac{1}{m}\sum_{i=1}^{m} f(\mathbf{u_i}, x_{ij}) f(\mathbf{v_i}, x_{ij}) - \hat{f}_0^2 \tag{2.24}$$

$$\hat{D}_{\sim j} = \frac{1}{m}\sum_{i=1}^{m} f(x_{ij}, \mathbf{u_i}) f(x'_{ij}, \mathbf{u_i}) - \hat{f}_0^2 \tag{2.25}$$

where the dimension of $\mathbf{u}$ and $\mathbf{v}$ is same to the dimension of ($\mathbf{x}$ - 1). New samples of input variables are used for $[\mathbf{u}, x_j]$ except x_j which is same as x_j in $\mathbf{x}$. $[x'_j, \mathbf{u}]$ uses same samples to $[\mathbf{u}, x_j]$ except x_j which is newly sampled. Usually, the functional form, $f(x)$, is scaled in the computation to have small f_0 because large f_0 results in the loss of accuracy. Using $f(x) - c_0$, where $c_0 \approx f_0$, is one of simple scaling ways suggested in [44].

Theoretical computational effort of the global sensitivity analysis is same as the effort of VABO Monte Carlo analysis but it requires more iterations to converge. Correlations of samples in the global sensitivity simulation slow the convergence rate [9].

2.4.2 Alternative Integral Representation

An alternative integral form for the total sensitivity is shown in Equation 2.26 [45]. This form enables the calculation of the total sensitivity from direct integrals of samples instead of the subtraction of the global sensitivity, $S_{T_j} = 1 - S_{\sim j}$.

$$S_{T_j} = \frac{1}{2}\frac{1}{D}\int [f(x_j, \mathbf{u}) - f(x'_j, \mathbf{u})]^2 d\mathbf{x} d\mathbf{u} \tag{2.26}$$

Monte Carlo integral estimation is,

$$\hat{S}_{T_j} = \frac{1}{2m}\frac{1}{\hat{D}}\sum_{i=1}^{m} [f(x_{ij}, \mathbf{u_i}) - f(x'_{ij}, \mathbf{u_i})]^2 \tag{2.27}$$

Global sensitivity also can be calculated from this integral approach.

$$\hat{S}_{T_{\sim j}} = \frac{1}{2m}\frac{1}{\hat{D}}\sum_{i=1}^{m} [f(\mathbf{u_i}, x_{ij}) - f(\mathbf{v_i}, x_{ij})]^2 \tag{2.28}$$

$$S_j = 1 - S_{T_{\sim j}} \tag{2.29}$$

This alternative integral approach is useful for the total sensitivity because the variance of total sensitivity with the alternative approach is smaller than the variance of total sensitivity with the method in Section 2.4.1. In the global sensitivity case, however, the variance of global sensitivity with the Section 2.4.1 method is smaller than those with alternative approaches. The proof of this comparison of variance is available in [45].

2.5 Summary

Different types of uncertainty assessment methods were introduced in this chapter. They are classified into a local sensitivity analysis or a global sensitivity analysis as well as into a deterministic method or a statistical method. The nominal range sensitivity analysis (NRSA) is a local and deterministic analysis. It is simple and fast in computation. However, this method cannot capture interaction effects because it assesses the effect of a variable on an output individually. The Hybrid Monte Carlo (HMC) sensitivity analysis is a method using both deterministic and probabilistic variables. This method has an advantage of assessing variables which cannot be represented statistically, such as assumptions and choices, while keeping other variables probabilistic. The Monte Carlo regression analysis is a useful method for screening influential variables. This method assesses the contribution of variables to outputs based on a linear regression model. The VABO Monte Carlo analysis assesses the impacts of uncertainty in terms of the mean and variance shift compared to the best estimate values. The Global sensitivity analysis investigates the contribution of variables to a total variance. The sensitivity indices are assessed over uncertainty ranges globally not at a fixed point. The global sensitivity analysis can evaluate all orders of interaction effects as well as a main effect or the sum of all effects. All assessment methods except the Monte Carlo regression analysis require a series of simulations the same as the number of input variables.

Uncertainties in a system can be investigated with one or more uncertainty analysis methods. Analyses based on the Monte Carlo simulation are recommended over a deterministic method for a complex model. For example, uncertainty of the APMT which includes 5 different blocks, where each block has several modules, can be assessed with statistical methods based on the Monte Carlo simulations. The random sampling from

probabilistic distributions also enables the propagation of uncertainty through modules and the evaluation of how the uncertainty in one module affects other modules. The next two chapters provide the implementation of these uncertainty and sensitivity analysis methods in two different modules of the APMT.

Chapter 3

Aircraft Price Model

3.1 Model Description

The aircraft price module estimates aircraft price from aircraft characteristics such as number of seats and maximum design range. Although there is a limitation that the model does not consider market conditions like demand and competition, it can provide generalized estimates of new aircraft price using performance characteristics. Two blocks, the regression block and the estimation block, compose the aircraft price module. The regression block builds the price model to relate aircraft price and performance based on historical data. Nonlinear least square regression is used to find the coefficients of a pre-defined function. The estimation block calculates aircraft price from the price model generated by the regression block with performance characteristics of the aircraft to be priced. Figure 3-1 shows the overview of the aircraft price module.

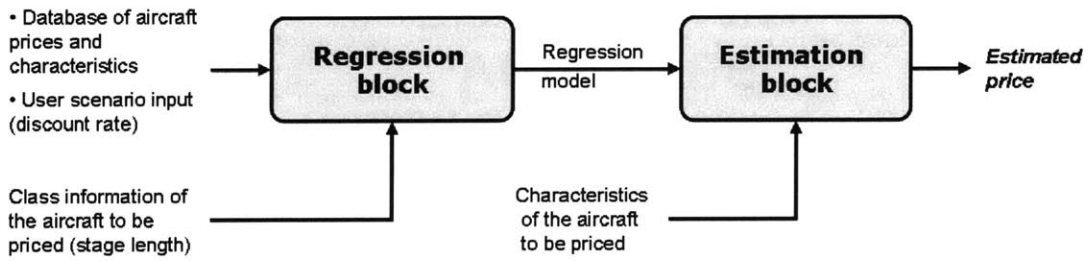

Figure 3-1: Overview of price module

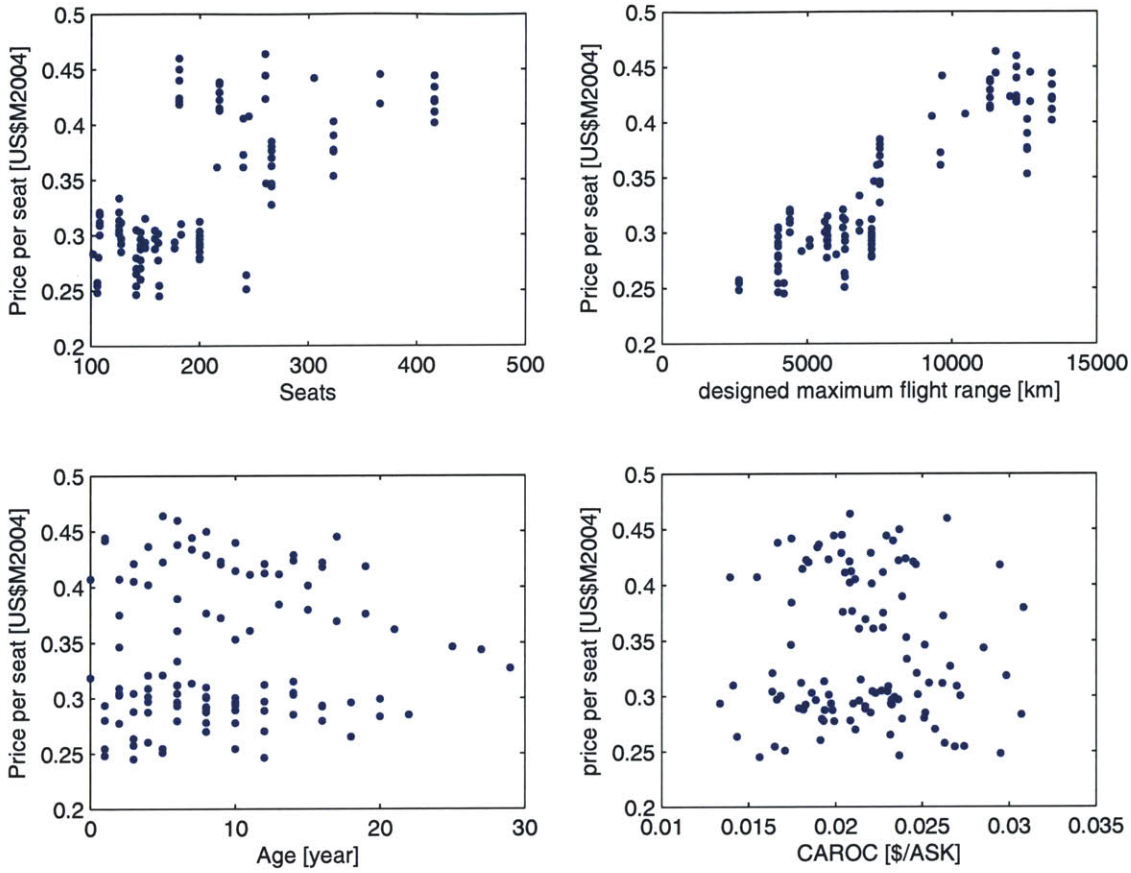

Figure 3-2: Relation between aircraft price and performance

3.2 Aircraft Database

Aircraft price data were based on Airline Monitor [31] from 1988 to 2004: a total 109 aircraft, 64 short-haul aircraft and 45 long-haul aircraft we considered. All data points come into the regression block at the same time to prevent capturing spurious relationships resulting from the small amount of data available in any one year. That is, data for the same aircraft in different years are recognized as different aircraft, while the price is discounted to current year or a specific year. Aircraft performance data are based on the aircraft specifications provided by manufacturers. These performance data include seats, maximum design range, year of introduction, and lifetime. Cash Airplane-Related Operating Costs (CAROC), stage length, annual trips, and fuel costs are obtained from the US Department of Transportation Form 41. Figure 3-2 shows discounted aircraft price per seat from all available data in Airline Monitor data from 1988 to 2004 with the performance data in the x-axis. Figure 3-2 suggests that there are two possible groups whose average price per

seat is different, about $0.4 millions and $0.3 millions each. However, aircraft in different groups show similar performance characteristics except maximum design range although their prices are different. This makes inaccurate regressions by capturing the relation of these two groups not the trend across individual aircraft. One of approaches to address this problem is a piecewise regression with different classes of aircraft. The detailed regression method is explained in the following section.

3.3 Model Development

Jacob Markish developed a price model as a function of seats, design range, and CAROC [29]. Markish's model is relatively simple and robust with few data points. The CAROC means Cash Airplane-Related Operating Costs, which include fuel cost and maintenance cost, and it reflects the preference of owners. The aircraft price model is based on the Markish's model, but introduces an additional independent variable, age, to enhance the regression statistics. The price regression model is shown in Equation 3.1.

$$\frac{Price}{seats} = \left[r_1 + r_2\left(\frac{max\_range}{\|max\_range\|}\right)\right] + k_1\left(\frac{seats}{\|seats\|}\right)^{\alpha} + k_2 \exp\frac{age}{\|age\|} + X_i k_3 f(CAROC) \tag{3.1}$$

$$where \qquad X_i = \begin{cases} 0 & \text{if } max\_range < 7500\,km \\ 1 & \text{if } max\_range \geq 7500\,km \end{cases}$$

All independent variables except the maximum range are used in the piece-wise regression model. As shown in Figure 3-2, aircraft in the database can be divided into two groups by price per seat. While the ranges of age and CAROC are not significantly different from each group and seats have a common range, maximum range has different values for each group. Therefore, maximum range is the most appropriate basis for dividing the groups. Two groups are short-haul aircraft, where the maximum range is smaller than 7500km and long-haul aircraft, where the maximum range is equal or larger than 7500km. Since the slope of the maximum range regression is similar in both groups and a similar linear pattern is shown across all aircraft, regression of maximum range was conducted with all aircraft at first apart from other independent variables. That is, r_1 and r_2 in the Equation 3.1 are calculated with all available aircraft data in the different regression process to regression

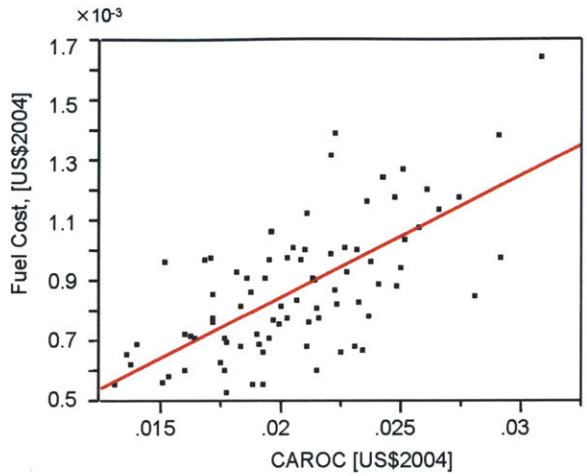

Figure 3-3: Linear fit of CAROC and fuel cost

of k_1, k_2, k_3 and α which are calculated with aircraft in one group piecewise. Regression of maximum range with all aircraft relaxes a discontinuity near the boundary of groups as well as captures a rising tendency in price as maximum range increases. After calculating r_1 and r_2, k_1, k_2, k_3 and α are calculated with a nonlinear least squares method while r_1 and r_2 are fixed at the precalculated value.

3.3.1 CAROC Regression

Since all aircraft data in different years were used in the regression at the same time by discounting dollars, CAROC values were converted to 2004 dollars as was aircraft price. However, when considering the CAROC of different years, the effect of fuel price on fuel cost should be considered in addition to the dollar conversion because fuel cost per operation is one of the major costs of airplane operations. Fuel cost per average stage length is available in the U.S. DOT Form 41. Equation 3.2 shows how the effect of fuel price is considered in converting CAROC in year i to CAROC in 2004 dollars. Historical data of fuel price and the dollar conversion factor are shown in Table B.1. When fuel cost information is not available for some of aircraft in the database, it is estimated from a linear regression function of CAROC and fuel cost. Figure 3-3 shows the linear relationship between CAROC and fuel cost. The regression function and summary of fit are shown in Table A.1.

$$\begin{aligned}\left\{(CAROC)_{i\,2004\$}\right\}_{\text{converted}} = (CAROC)_{i\,2004\$} + \\ + \left(\frac{(fuel\ price)_{2004\,2004\$}}{(fuel\ price)_{i\,2004\$}} - 1\right) \times (fuel\ cost)_{i\,2004\$}\end{aligned} \tag{3.2}$$

Markish used the lifecycle cost increment, which is a function of CAROC, instead of direct CAROC because of the correlation between CAROC and aircraft size. The lifecycle cost increment is calculated as Equation 3.5. In Equation 3.4, $CAROC_{\text{actual}}$ is the CAROC value of an aircraft in the database converted to the 2004 dollars, and $CAROC_{\text{nominal}}$ is the expected CAROC value calculating from a first order linear regression function in Equation 3.3 with aircraft seats. Although Markish applied the model to two different classes of aircraft based on the size – narrow body or wide body, CAROC regression in this thesis used aircraft class based on maximum range – long-haul aircraft or short-haul aircraft – to keep the consistency with the piecewise regression.

$$CAROC_{\text{nominal}} = p_1 \times (seats) + p_2 \tag{3.3}$$

$$\Delta CAROC = CAROC_{\text{actual}} - CAROC_{\text{nominal}} \tag{3.4}$$

$$\Delta LC = \Delta CAROC \times (seats) \times (annual\ trips) \times (stage\ length) \times (discount\ factor) \tag{3.5}$$

where $$discount\ factor = \frac{1}{1+(discount\ rate)} \times \left[\frac{1-\left(\frac{1}{1+(discount\ rate)}\right)^{(service\ life)}}{1-\left(\frac{1}{1+(discount\ rate)}\right)} \right]$$

ΔLC = the lifecycle cost increment

$annual\ trips$ = the number of averaged trips per year

$stage\ length$ = the average length per one stage

$service\ life$ = the assumed average ages until retirement

Generally, it is expected that the high lifecycle cost increment decreases the aircraft price because the price the buyer is willing to pay will decrease as the lifecycle cost increment increases. Figure 3-4(b) shows that this negative relation between the lifecycle cost increment and aircraft price is significant in the long-haul aircraft class ($p = 0.0220$). In contrast, there are no significant relations between aircraft price and the lifecycle cost increment in the short-haul aircraft class ($p = 0.8776$) as shown in Figure 3-4(a). Fitting results are summarized in Table A.2 and Table A.3. Therefore, when the aircraft to be priced belongs to the short-haul aircraft class, the CAROC term is dropped in the regression model by in-

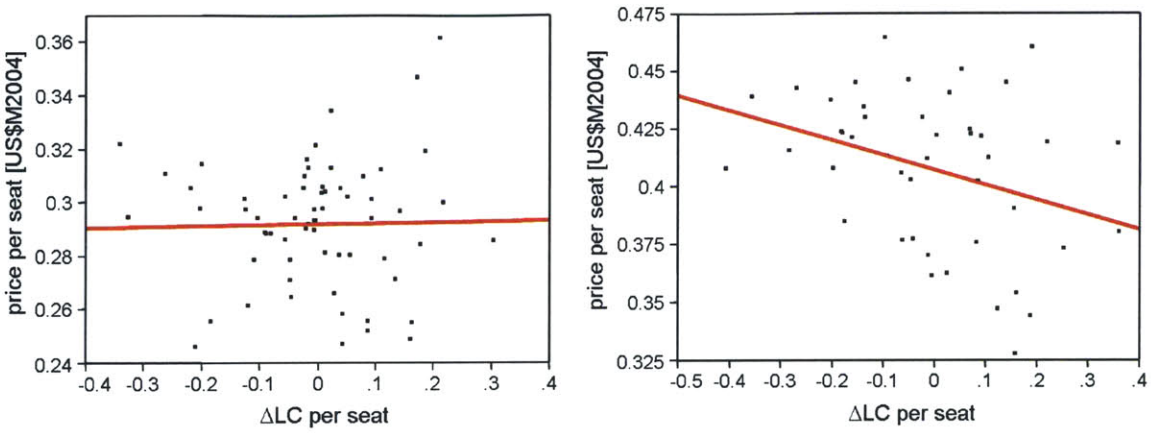

(a) Short-haul aircraft class

(b) Long-haul aircraft class

Figure 3-4: Fitting results between the lifecycle cost increment and the aircraft price

troducing additional indicator variable, X_i in Equation 3.1, to prevent improper regression.

3.4 Regression Result

Table 3.1 shows the regression result for maximum range. The coefficients of maximum range are significant with 95% confidence level for both aircraft classes. The regression coefficients of maximum range were estimated with all possible aircraft data, and these coefficients are common for both classes. Table 3.2 shows the regression results of a short-haul aircraft class and a long-haul aircraft class and the coefficients of seats, age, and ΔLC. The regression block selects the appropriate aircraft class according to the maximum range of the aircraft to be priced. If the selected class is a short-haul aircraft, ΔLC is dropped. Figure 3-8 shows the regression result: actual price versus estimated price of aircraft used in the regression. Duplicate aircraft are shown in Figure 3-8 because all available aircraft were used in the regression at the same time. As a result, the price module overestimates the aircraft price by about 3% because of decreasing aircraft price trend as shown in Figure 3-9. Figure 3-5, Figure 3-6, and Figure 3-7 show the profilers of regression for input variables and regression coefficients, which plot the change of price per seat as varying one input variable at a time. The profiler plots show that age effect on the price per seat is not significant and regression coefficients of seats, k_1 and α, are sensitive around the estimated point. The sensitivity analysis in the following section will confirm the result in this profilers plot.

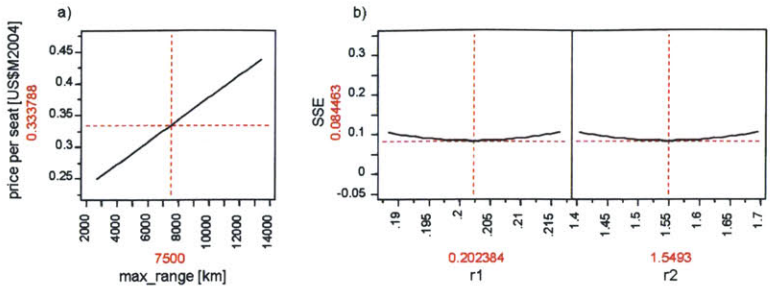

Figure 3-5: Profilers of maximum range regression: a)Prediction profiler b)Profiler-SSE

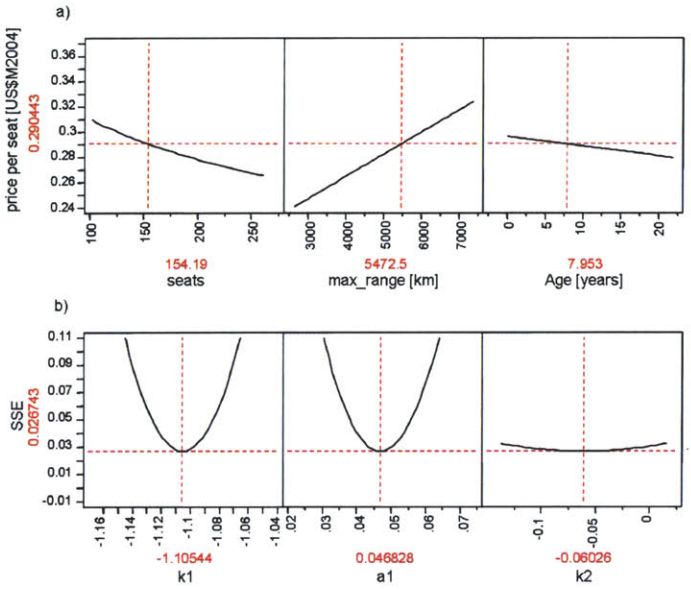

Figure 3-6: Profilers of price model regression for short-haul aircraft: a)Prediction profiler b)Profiler-SSE

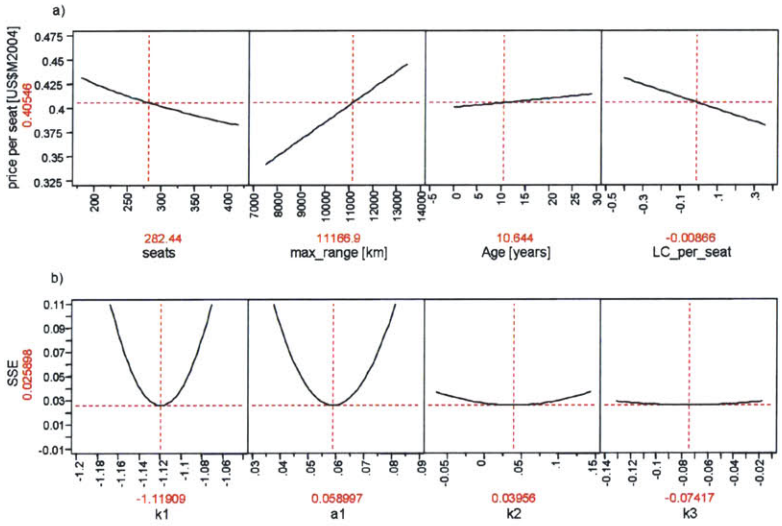

Figure 3-7: Profilers of price model regression for long-haul aircraft: a)Prediction profiler b)Profiler-SSE

	SSE	DF	MSE	RMSE
	0.08446	107	0.0007894	0.02810
Parameter	Estimate	Lower CL	Upper CL	Std.Err.
r_1	0.2024	0.1885	0.2163	0.007023
r_2	1.5493	1.4039	1.6947	0.07332

Table 3.1: Regression result of maximum range

Short-haul aircraft class:

	SSE	DF	MSE	RMSE
	0.02674	61	0.0004384	0.02094
Parameter	Estimate	Lower CL	Upper CL	Std.Err.
k_1	-1.1054	-1.1633	-1.0501	0.02831
α_1	0.04683	0.02366	0.06990	0.01156
k_2	-0.06026	-0.1380	0.01592	0.03849

Long-haul aircraft class:

	SSE	DF	MSE	RMSE
	0.02590	41	0.0006317	0.02513
Parameter	Estimate	Lower CL	Upper CL	Std.Err.
k_1	-1.1191	-1.1843	-1.0570	0.03144
α_1	0.05900	0.0303	0.08772	0.01418
k_2	0.03956	-0.06758	0.1432	0.05203
k_3	-0.07417	-0.1316	-0.01678	0.02840

Table 3.2: Regression result of price model

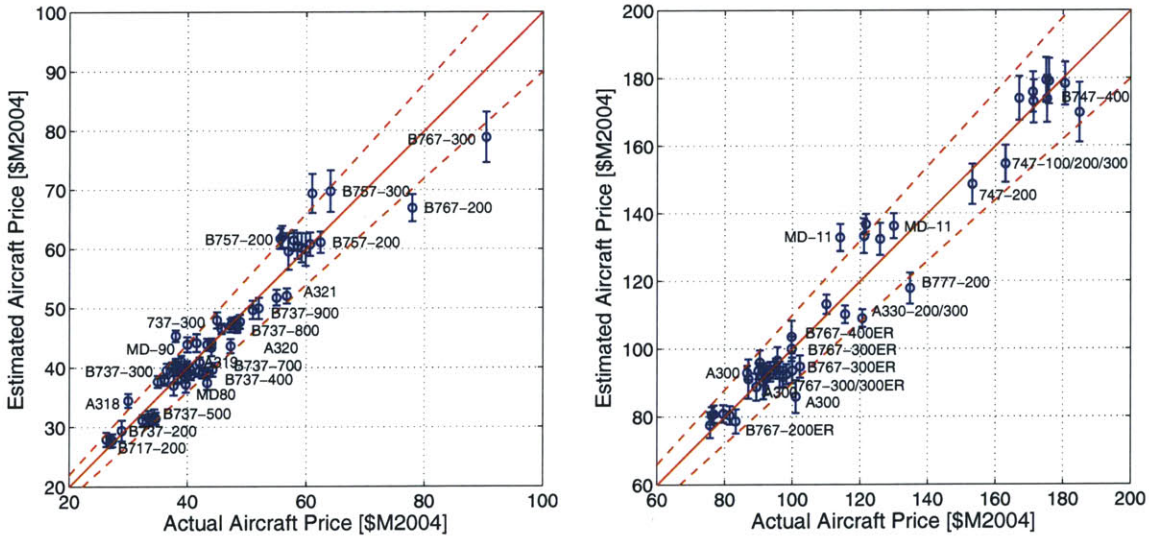

(a) Short-haul aircraft

(b) Long-haul aircraft

Figure 3-8: Aircraft price estimation

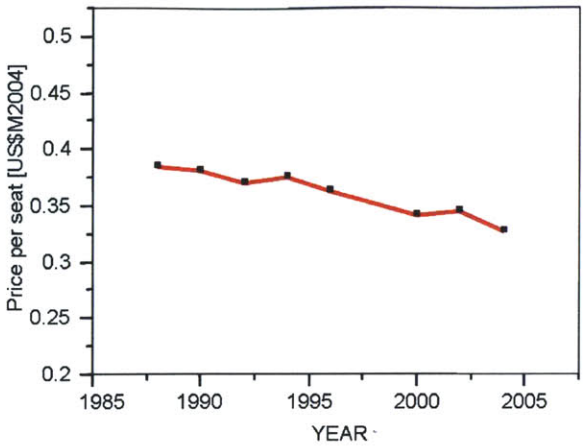

Figure 3-9: Price trend of A300 from 1988 and 2004

3.5 Uncertainty Assessment

Monte Carlo simulations in the uncertainty assessment did not include the uncertainty of aircraft in the database. Instead, the uncertainty propagation starts from the regression coefficient. That is, the analysis does not vary the database directly but varies the regression coefficient based on the confidence intervals to capture the uncertainty of database. This approach makes it possible to increase the number of iterations by decreasing the running time of one iteration of the Monte Carlo simulation. To ensure this approach is valid for representing the uncertainty in the database, a Monte Carlo simulation with 1000 iterations was conducted by varying the aircraft database within 10% uniformly. Figure 3-10 shows the result distribution of regression coefficients and the 95% confidence intervals of the regression with deterministic database. Overall estimated intervals are not much different from the distribution result. In addition to the regression coefficients, the uncertainty in the aircraft performance to be priced is investigated. All uncertainty assessments were conducted with separate aircraft classes.

3.5.1 Input Distribution

Two aircraft examples belonging to each aircraft class are selected for an input of uncertainty assessment: 737-800 for short-haul aircraft and 767-300ER for long-haul aircraft. Table 3.3 shows the performance characteristics of the two aircraft and their upper and lower bound of input distribution used in these analyses. Bounding values were simply set to $\pm 10\%$ of the base value for maximum range, age, and lifetime, $\pm 20\%$ for annual trips and stage length,

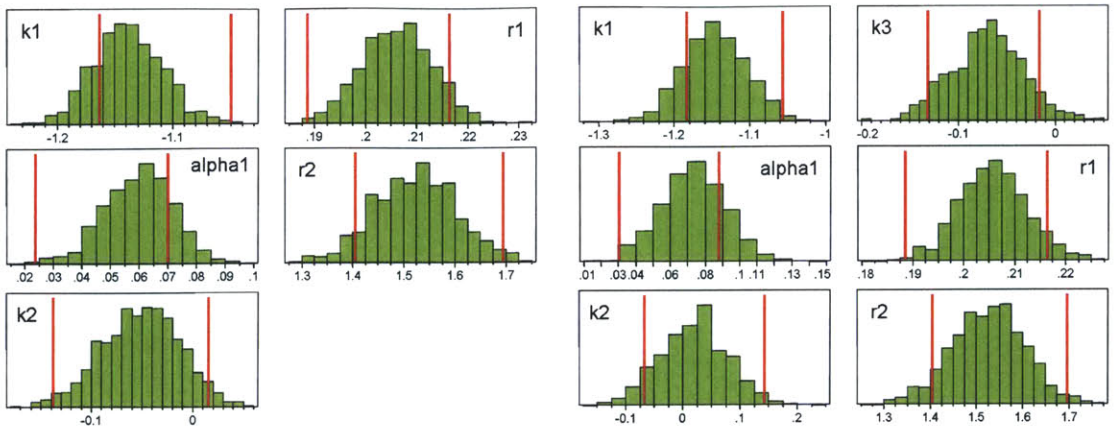

(a) Short-haul aircraft

(b) Long-haul aircraft

Figure 3-10: Distribution result of uniformly varied database within 10%

		seats	maximum range $[km]$	year of entry	CAROC [\$/ASK]	lifetime $[years]$	annual trips	stage length $[km]$
737-800	base	162	5670	1998				
	UB	197	6237	1999				
	LB	162	5103	1997				
767-300ER	base	218	11306	1988	0.023617	27	834	3863
	UB	279	12437	1990	0.029521	37	1002	4635.6
	LB	218	10175	1986	0.017713	27	668	3090.4

where base is actual value of aircraft performance in Airline Monitor 2004,
UB is the upper bound value and LB is the lower bound value.

Table 3.3: Aircraft performance characteristics

and ±25% for CAROC. For the seats distribution, the bounds were set based on structural variability of seats in aircraft. Airliners control the number of seats in the aircraft according to their benefit, for example, they set maximum seats when all seats are used for economy class. To estimate the influence of seats variability, 17 aircraft of Boeing and Airbus were used in the regression between most-likely values and the normalized difference of bound values and a most-likely value of seats. Figure 3-11 shows the fitting result, and Table A.4, A.5, A.6, and A.7 show summary of fitting statistics. As shown in Figure 3-11, large aircraft and small aircraft show different seat variability. For example, the number of seats installed most-likely is close to the lower limit of the number of seats in large aircraft. The lower and upper bounds of seats distribution estimated based on the structural seats variability will be in the range which is more plausible in real aircraft. Beta distributions with the bounds in Table 3.3 were used for aircraft performance variables and uniform distributions with the

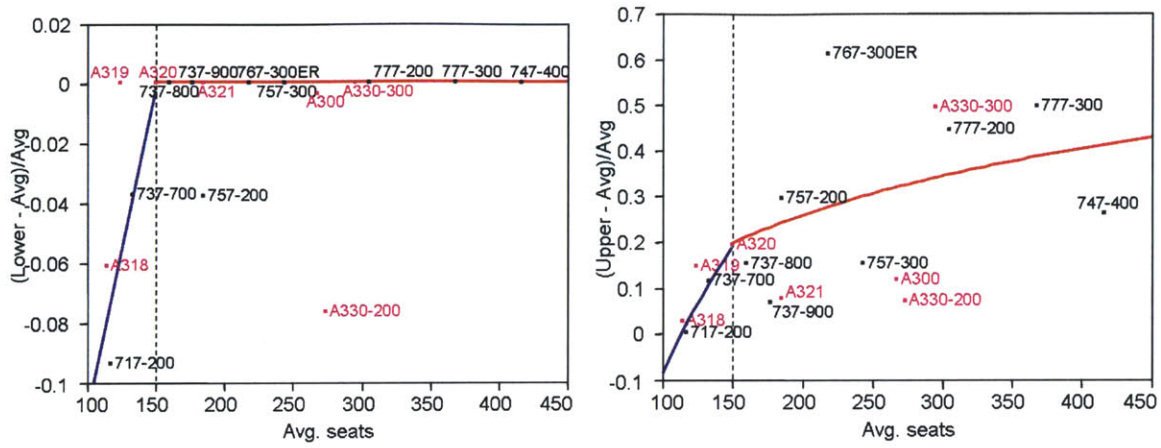

(a) Small seat class ($\leq$ 150 seats)

(b) Large seat class ($>$ 150 seats)

Figure 3-11: Fitting results of lower and upper values of seats

95% confidence interval were used for the regression coefficients in the random sampling of Monte Carlo simulations.

3.5.2 Convergence Error

To determine whether the variance comes from the uncertainty of the input variable or the Monte Carlo simulation itself, it is necessary to check the convergence error of the Monte Carlo simulation and increase the number of iterations to decrease convergence error. If the contribution of a parameter is smaller than convergence error of the Monte Carlo simulation, one cannot identify whether the effect comes from the parameter or simulation error. Convergence error was calculated from mean and variance distributions where normal distributions were assumed. Convergence error is set as the % difference between the 95% confidence interval of mean or variance and the estimated value, as shown in Equation 3.6. Convergence error is 0.1% for the mean shift and 0.9% for the variance shift with 100000 iterations for the VABO Monte Carlo simulation, and 0.6% for the variance shift with 200000 iterations for the global sensitivity simulation.

$$\text{Convergence error} = \frac{[\text{variance or mean}] \text{ of output} - \text{lower CI}}{[\text{variance or mean}] \text{ of output}} \tag{3.6}$$

Figure 3-12 and Figure 3-13 compare four different approaches of global sensitivity analysis. The normalized approach, $f(x) - c_0$, is most stable for the Sobol's index, and the normalized alternative approach in section 2.4.2 is most stable for the total sensitivity

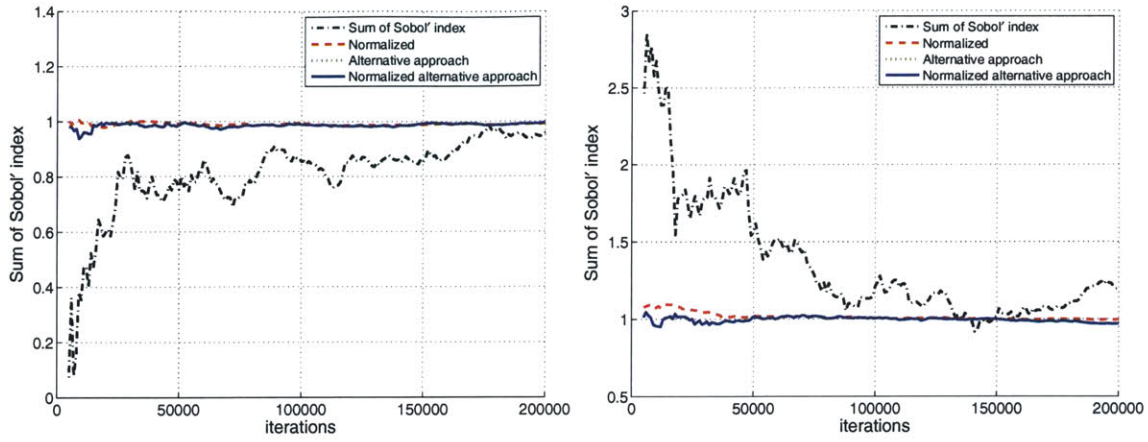

(a) Short-haul aircraft (b) Long-haul aircraft

Figure 3-12: Convergence history of sum of Sobol's indices

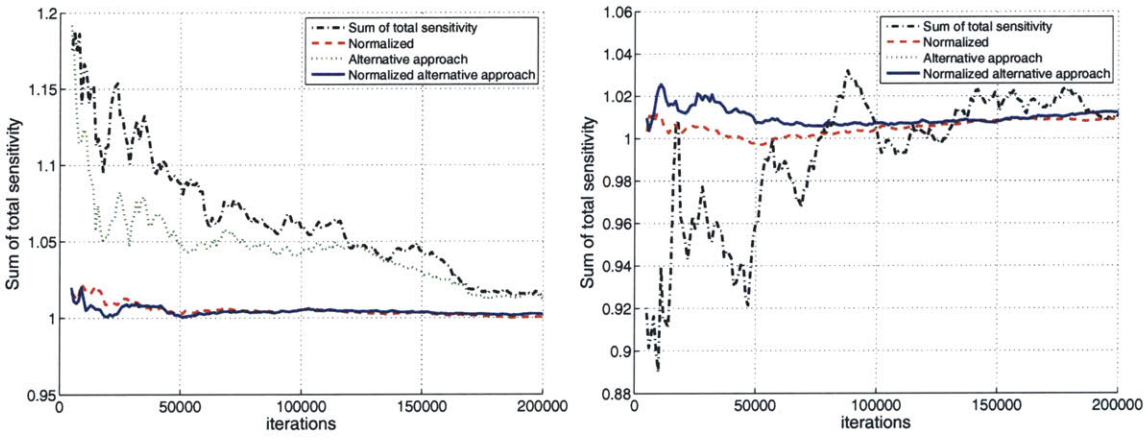

(a) Short-haul aircraft (b) Long-haul aircraft

Figure 3-13: Convergence history of sum of total sensitivities

analysis. Therefore, the normalized approach and normalized alternative approach were used for calculating the Sobol's index and the total sensitivity of each.

3.5.3 Nominal Range Sensitivity Analysis

The Nominal Range Sensitivity Analysis (NRSA) investigates the contribution of parameters to the mean shift of price by shifting one parameter to its bound value at a time. Figure 3-14(a) shows sensitivities of parameters in short-haul aircraft. Aircraft price is most sensitive to seats coefficients and the number of seats, and it is not sensitive to the age. This result agrees with the profiler plots in the section 3.4. Aircraft price becomes more sensitive to the number of seats and seats coefficients in the price estimation than the

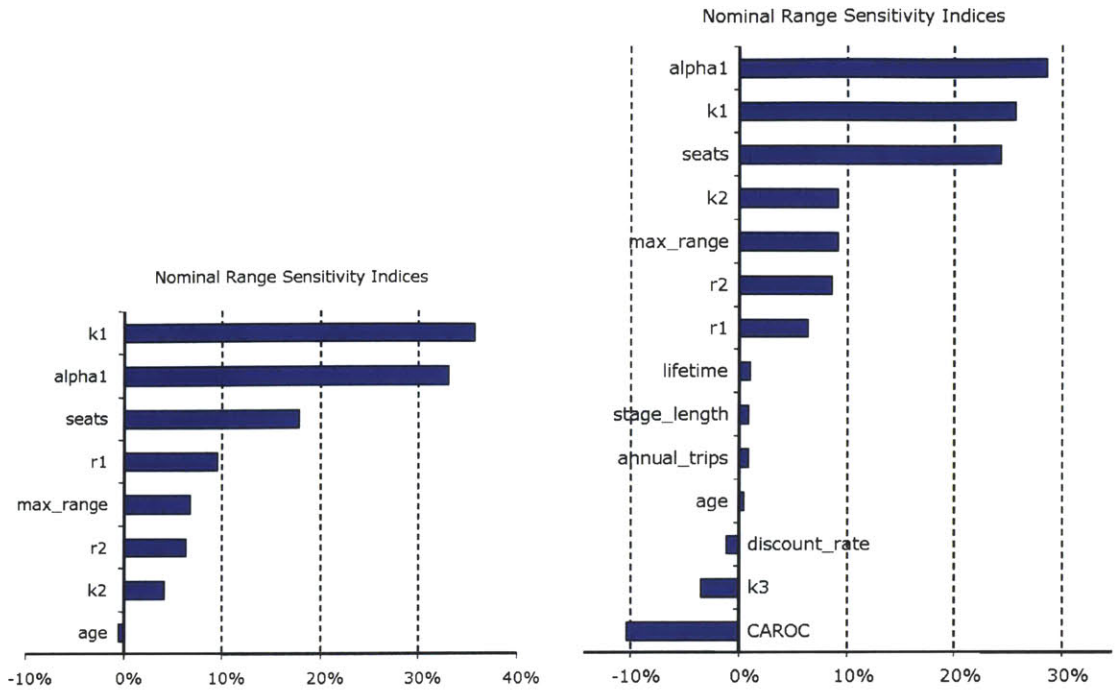

(a) Short-haul aircraft

(b) Long-haul aircraft

Figure 3-14: Sensitivity result

price per seat estimation which the profiler plots show because seats are multiplied by price per seat to calculate the price. In the long-haul aircraft shown in Figure 3-14(b), price is most sensitive to the number of seats and the coefficients of seats and not sensitive to the age like the short-haul aircraft case. CAROC and its coefficient have negative effects in the price estimation because of its negative relation with the price. Other variables involved in calculating the life cycle cost increment are not sensitive parameters. The sensitivity of the age coefficients, k_2, increases in the long-haul aircraft compared to the result of short-haul aircraft.

3.5.4 Monte Carlo Regression Analysis

Table 3.4 shows the standardized regression coefficients, Std. Beta in the table, of the first order regression model with 10000 iterations of the Monte Carlo simulation, where all coefficients are significant. Important parameters are screened based on these standardized regression coefficients. Large Std. Beta indicates the influential impact to the mean and variance shifts of a variable. In the aircraft price module, the regression coefficients of seats contribute to the mean shift and variability of aircraft price most significantly in both short-

Parameters	737-800			767-300ER		
		Contribution to			Contribution to	
	Std. Beta	Mean	Variance	Std. beta	Mean	Variance
seats	0.262	12.9%	7.0%	0.375	17.6%	14.1%
max_range	0.081	4.0%	0.7%	0.127	5.9%	1.6%
age	-0.006	-0.3%	0.0%	0.006	0.3%	0.0%
CAROC	-	-	-	-0.147	-6.9%	2.2%
lifetime	-	-	-	-0.009	-0.4%	0.0%
annual trips	-	-	-	-0.007	-0.3%	0.0%
stage length	-	-	-	-0.006	-0.3%	0.0%
discount rate	-	-	-	0.013	0.6%	0.0%
k_1	0.684	33.8%	47.7%	0.582	27.2%	33.9%
α_1	0.620	30.6%	39.1%	0.617	28.9%	38.1%
k_2	0.079	3.9%	0.6%	0.206	9.6%	4.2%
k_3	-	-	-	0.044	2.1%	0.2%
r_1	0.182	9.0%	3.4%	0.145	6.8%	2.1%
r_2	0.121	6.0%	1.5%	0.190	8.9%	3.6%

Table 3.4: Result of Monte-Carlo regression analysis

haul and long-haul aircraft classes. Overall ranking of important parameters is similar in both aircraft classes. Table A.8 and Table A.9 show the fitting result of the regression.

3.5.5 Vary-all-but-one Monte Carlo Analysis

Table 3.5 shows the % shift of mean and variance to the all varying case with the vary-all-but-one (VABO) Monte Carlo simulation. The uncertainty of a parameter was removed from the full varying Monte Carlo simulation by fixing the parameter at its base value shown in Table 3.1, 3.2, and 3.3 while varying the other parameters with distributions. Significant results larger than the convergence error, 0.1% for the mean shift and 0.9% for the variance shift, have an asterisk next to the number. The mean shift results show there is no significant bias of estimation caused by parameter uncertainties and most parts of mean bias are contributed from performance variables of aircraft. On the other hand, the uncertainty in the regression coefficients of seats contribute to the variability of the price significantly but not to the mean bias. That is, the estimation of price is most sensitive to the seats coefficients, but the response is not skewed. CAROC in long-haul aircraft contributes to the mean shift as a similar amount as with other input variables such as seats and maximum range, but does not contribute to the variability of output significantly.

	737-800		767-300ER	
Case	Mean [2003$M]	Variance [2003$M]	Mean [2003$M]	Variance [2003$M]
All varying	50.2	57.9	98.7	178.5
Actual value	47.5	-	92	-
Parameters	% Mean shift	% Variance shift	% Mean shift	% Variance shift
Actual value	-5.5%	-	-6.7%*	-
seats	-5.6%*	-17.9%*	-7.2%*	-26.2%*
max_range	-3.4%*	-1.6%*	-4.8%*	-3.7%*
age	0.3%*	-0.6%	-0.2%*	-0.7%
CAROC	-	-	5.4%*	0.7%
lifetime	-	-	0.4%*	-0.6%
annual trips	-	-	0.2%*	-1.3%*
stage length	-	-	0.1%*	-1.5%*
discount rate	-	-	-0.0%	-0.7%
k_1	0.0%	-48.7%*	0.0%	-33.4%*
α_1	0.2%*	-38.9%*	0.1%	-38.5%*
k_2	0.0%	-0.8%	-0.1%	-4.2%*
k_3	-	-	-0.1%	-1.2%*
r_1	0.0%	-3.9%*	0.0%	-2.2%*
r_2	0.0%	-2.3%*	0.0%	-4.4%*

Table 3.5: Result of Vary-all-but-one Monte Carlo Analysis

	737-800		767-300ER	
Parameters	Sobol' index	Total sensitivity	Sobol' index	Total senstivity
seats	6.8%*	7.1%*	13.8%*	14.3%*
max_range	0.6%*	0.7%*	1.5%*	1.6%*
age	-0.3%	0.0%	-0.4%	0.0%
CAROC	-	-	2.5%*	2.7%*
lifetime	-	-	-0.1%	0.0%
annual trips	-	-	0.3%	0.0%
stage length	-	-	0.4%	0.0%
discount rate	-	-	0.0%	0.0%
k_1	48.3%*	48.2%*	33.1%*	33.8%*
α_1	38.7%*	38.5%*	38.0%*	38.0%*
k_2	0.5%	0.7%*	4.4%*	4.3%*
k_3	-	-	0.1%	0.6%*
r_1	3.0%*	3.4%*	2.2%*	2.1%*
r_2	1.3%*	1.5%*	4.0%*	3.7%*

Table 3.6: Result of Global Sensitivity

Parameters	737-800 NRSA	MC	VABO	Sobol'	Total	767-300ER NRSA	MC	VABO	Sobol'	Total
seats	3	3	3	3	3	3	3	3	3	3
max_range	5	6	6	6	6	6	8	6	8	8
age	8	8	7	7	8	14	12	11	9	10
CAROC	-	-	-	-	-	4	6	11	6	6
lifetime	-	-	-	-	-	10	11	14	12	10
annual trips	-	-	-	-	-	12	12	9	11	10
stage length	-	-	-	-	-	12	12	8	9	10
discount rate	-	-	-	-	-	11	10	11	14	10
k_1	1	1	1	1	1	2	2	2	2	2
α_1	2	2	2	2	2	1	1	1	1	1
k_2	7	7	8	6	6	5	4	5	4	4
k_3	-	-	-	-	-	9	9	10	12	9
r_1	4	4	4	4	4	8	7	7	7	7
r_2	6	5	5	5	5	7	5	4	5	5

Table 3.7: Rank comparison of uncertainty assessment results

3.5.6 Global Sensitivity

Table 3.6 shows two different global sensitivity indices, Sobol' and total sensitivity. Significant results larger than the convergence error, 0.6%, have an asterisk next to the number. The regression coefficients of seats contribute to most part of variability in the output and the age is not a significant input variable. Also, the contribution of the age coefficient increases in the long-haul aircraft as the VABO result suggests. Interaction effects is investigated by comparing the rank of the Sobol index, which present the main effect only, to the rank of the total sensitivity, which present the sum of main and interaction effects. Similar rank and the similar magnitude of two indices suggest that there are no significant interactions. However, precise comparison of the Sobol' index and the total sensitivity is not available because the convergence rates of the two indices are different.

3.6 Conclusion

Table 3.7 compares the rank of parameters of five different uncertainty assessment methods. The results closely agree with each other. The coefficients of seats contributes to the uncertainty most significantly. The contribution of the number of seats is also significant, but age is most insignificant between independent variables of the price model. Similar ranking between the Sobol' indices and the total sensitivity indices shows that there are

no significant interactions. While overall magnitude of indices is approximately similar in the VABO Monte Carlo analysis and the global sensitivity analysis, but the result of the seats is greater in the VABO Monte Carlo analysis because of nonlinearity related to seats. Also, the lower rank of CAROC in the VABO Monte Carlo analysis suggests that CAROC value near its base value decreases the variability. These very similar results from different uncertainty assessment methods suggest that a simple method, such as the NRSA or the Monte Carlo regression analysis, can provide acceptable results when assessing a simple model. In the simple aircraft price module described above, for example, the results of the contribution to variance in the Monte Carlo regression analysis almost agree with the results in the total sensitivity indices. However, simple methods may not be preferable if a model has nonlinearity or significant interactions.

Chapter 4

Climate Model

The climate module can assess the environmental and socio-economic impact of aircraft emissions. Greenhouse gases (GHG) like CO_2 from carbon emissions of aircraft remain in the atmosphere and increase the surface temperature related potentially leading to increased costs, such as restoring costs from climate diasters, changes in farming production and other consequences. Among many different possible metrics for representing the climate impact of aviation, this paper uses three different metrics as outputs of the climate module: the globally averaged surface temperature changes, damage as a percentage impact on GDP, and Net Present Value (NPV) as dollars. The climate module can be used for assessing the aviation growth scenarios, the effect of background anthropogenic emissions, or policy impacts. Also, uncertainty propagation in the physical and economic climate parameters can be assessed by Monte Carlo simulations with the climate module.

4.1 Model Structure

Figure 4-1 shows the overview of the modeling approach of the climate module following the approaches of Hasselmann et al. (1997) [17], Sausen and Schumann (2000) [40], Fuglestvedt et al. (2003) [13], Shine et al. (2005) [42] and Nordhaus and Boyer (2000) [36]. When calculating the physical climate impacts like radiative forcing and global surface temperature changes, the climate module use simple impulse response functions instead of complex energy exchange models like those in a general circulation model (GCM). Section 4.2.1 and Section 4.2.1 will explain the details of the impulse response functions and coefficients. The climate impact block and impact valuation block compose the climate module which takes

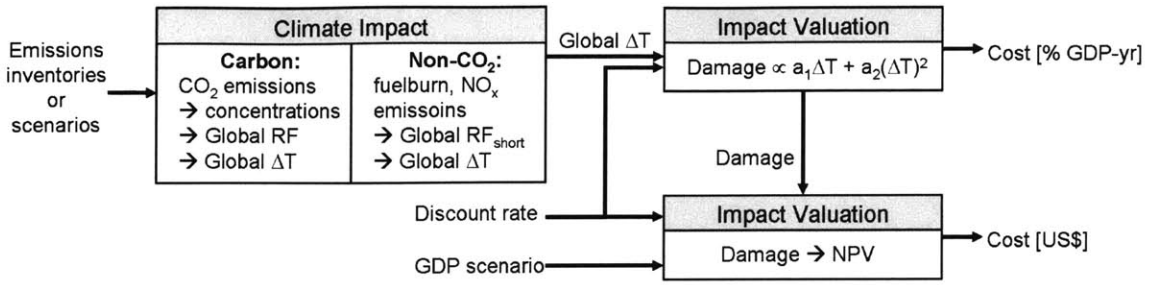

Figure 4-1: Overview of climate module

emissions inventories or scenarios as inputs and generates the globally averaged surface temperature change, damage, and cost as outputs. The climate impact block processes the effect of carbon emissions and non-CO_2 emissions separately with different approaches, where CO_2 radiative forcing is calculated from its concentration but non-CO_2 radiative forcing is calculated from the emission index directly by scaling of CO_2 radiative forcing. The physical impacts of CO_2 and non-CO_2 are also different. CO_2 emissions remain in the atmosphere hundred years, but non-CO_2 emissions disappear rapidly compared to CO_2. For example, contrails and contrail-induced cirrus remain only a few hours or days and the effect of CH_4 induced by NO_x emissions remains about 10-30 years. The climate module assesses non-CO_2 emissions in terms of two effects, the effect of cirrus, sulfates, soot, water, and contrails come from fuel burn and the effect of ozone and methane creation or destruction induced by NO_x emissions. There are two modes in the ozone creation by NO_x emission. Ozone creation in the short mode disappears within one year while ozone destruction in the long mode has a same lifetime as CH_4.

In contrast to the CO_2 effect which is well understood physically, there are still significant uncertainties in the effects of non-CO_2 impacts such as aviation-induced cirrus [39]. To reflect uncertainties in the physical model such as climate sensitivity and radiative forcing of short-lived effects, inputs or internal coefficients are presented as probabilistic distributions. Assumptions like a aviation scenario or discount rate are treated as selectable options.

4.2 Physical Climate Impact

4.2.1 Impact of Carbon Emission

The CO_2 impact should be calculated with considering background CO_2 concentrations because of a very long residence time, approximately 300 years. The climate module calcu-

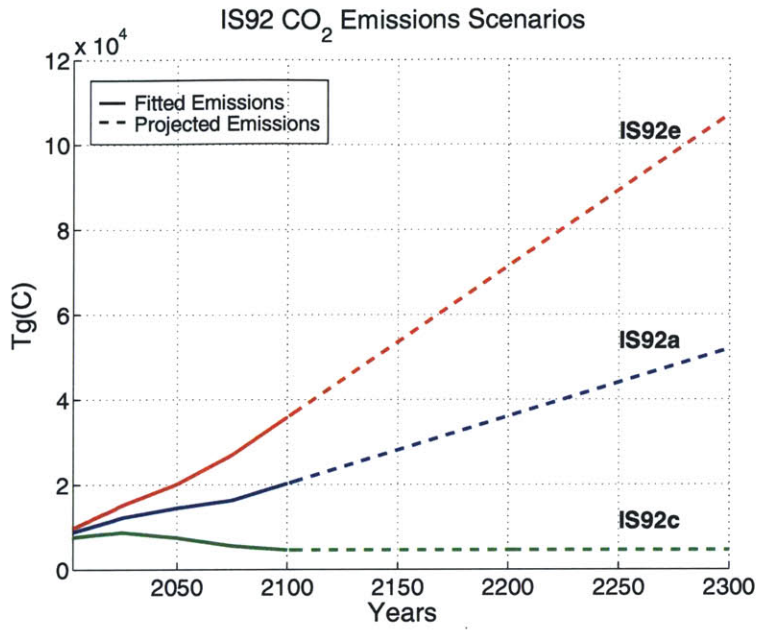

Figure 4-2: IS92 Emission Scenarios

lates the impact of aviation CO_2 relative to total anthropogenic carbon emissions. That is, the impact of aviation CO_2 is determined by subtracting all anthropogenic CO_2 excluding aviation CO_2 from all anthropogenic CO_2 including aviation CO_2. IS92 scenarios of Intergovernmental Panel on Climate Change (IPCC) are used for the background anthropogenic carbon concentration up to 2100. After 2100, the scenario for background carbon emission is extended up to the end of simulation years by extrapolating. For the IS92c, declining carbon emission scenario, the emissions are assumed to remain the same level of 2100 emission after 2100 not to be negative level. Figure 4-2 shows the background emission level of three scenarios.

Aviation Emission

The climate module can take either one year emission inventories or scenario emissions as an input. This thesis uses a one year aviation emissions impulse based on 2003 data of the FAA Aviation Environmental Design Tool System for assessing Aviation's Global Emissions (AEDT/SAGE) [1][2]. For the aviation emission scenarios, 2003 AEDT/SAGE inventories, 2015 NASA estimation, and 2050 FESG scenarios (Fa1, Fc1, and Fe1) [5] are used with interpolation in years up to 2050. Following the assumption of Sausen and Schumann, 2000 [40], 1% growth per year is assumed after 2050 until 2100, and the aviation emission

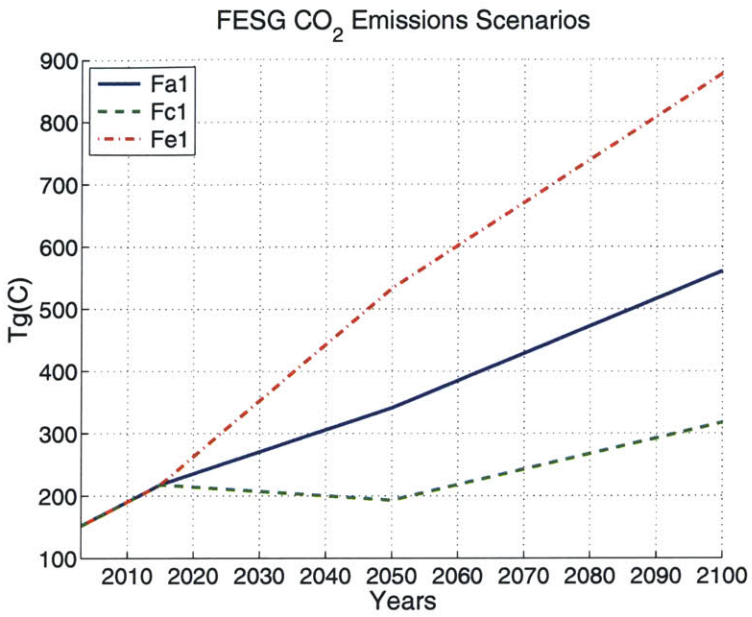

Figure 4-3: FESG Aviation Emissions Scenarios

scenarios are ended in 2100. Figure 4-3 shows three aviation scenarios used in this thesis.

CO_2 Concentrations

CO_2 concentration is calculated from impulse models of a carbon cycle using linearized impulse response functions in Equation 4.1 [17][40].

$$\begin{aligned} G_c(t') &= \sum_{j=1}^{n_j} \alpha_j e^{-(t')/\tau_j} \\ \Delta X_{CO_2}(t') &= \int_{t_0}^{t'} Q_{CO_2}(t'') \cdot G_c(t' - t'')dt'' \\ &\approx \sum_{n=0}^{N-1} Q_{CO_2}(t_0 + n\Delta t) \cdot G_c(t' - t_0 - n\Delta t) \cdot \Delta t \end{aligned} \tag{4.1}$$

where $N = (t' - t_0)/\Delta t$

G_c = the impulse response function of a carbon cycle

Q_{CO_2} = the mass of CO_2 emissions

ΔX_{CO_2} = the change of CO_2 concentration by Q_{CO_2}

Coefficients of carbon cycle impulse function†						Reference
α_j	0.132	0.311	0.253	0.209	0.095	Hooss et al. 2001 [22]
τ_j	inf	236.5	59.52	12.17	1.271	
α_j	0.067	0.1135	0.152	0.097	0.041	Hasselmann et al. 1993 [18]
τ_j	inf	313.8	79.8	18.8	1.7	
α_j	0.033	0.305	0.048	0.046	0.04	Hasselmann et al. 1997 [17]
τ_j	inf	258.5	71.9	17.6	1.6	
α_j	0.217	0.259	0.338	0.186		Plattner et al. 2001 [37],
τ_j	inf	172.9	18.51	1.186		Joos et al. 2001 [25]‡

†α: ppbv/TgC, τ: years, ‡Bern carbon cycle model

Table 4.1: Coefficients of Carbon Cycle Impulse Response Function

Table 4.1 shows several available sets of the coefficients of the carbon cycle impulse function, α and τ.

Radiative Forcing

Radiative forcing (RF) is a perturbation in the energy balance system of Earth by incoming and outgoing radiation at the atmosphere. Positive RF causes a warming effect and negative RF causes a cooling effect. A change in GHG concentrations results in a change of RF [24]. The climate module uses the normalized radiative forcing, which is a logarithmic function of CO_2 concentration, as shown in Equation 4.2. [40]

$$RF^*_{CO_2}(t') = \log_2\left(\frac{X_{CO_2(present)} + \Delta X_{CO_2}(t')}{X_{CO_2(1750)}}\right) \tag{4.2}$$

where $X_{CO_2(1750)} = 278$ ppmv [24] (a pre-industrial level of CO_2 concentration)

The normalized radiative forcing of CO_2 becomes 1 when the CO_2 concentration becomes double of the unperturbed level in 1750.

Temperature Change

Temperature change is determined from the normalized RF with a impulse response function of the temperature response model in Equation 4.3. Table 4.2 shows the coefficients of the

temperature response impulse function.

$$
\begin{aligned}
G_T(t) &= \sum_{i=1}^{n_i} \alpha_i e^{-(t)/\tau_i} \\
\Delta T_{CO_2}(t) &= \int_{t_0}^{t} RF^*_{CO_2}(t') \cdot G_T(t-t')dt' \\
&\approx \sum_{n=0}^{N-1} RF^*_{CO_2}(t_0 + n\Delta t) \cdot G_T(t - t_0 - n\Delta t) \cdot \Delta t
\end{aligned} \tag{4.3}
$$

where $N = (t - t_0)/\Delta t$

Coefficients of temperature response function†				Climate Sensitivity	Reference
α_i	0.290/400	0.710/12		2.39K	Hooss et al. 2001 [22]
τ_i	400	12			
α_i	1/36.8			2.5K	Hasselmann et al. 1993 [18]
τ_i	36.8				
α_i	0.484/2.1	0.3036/12	0.2124/138.6	2.5K	Hasselmann et al. 1997 [17]
τ_i	2.1	12	138.6		
α_i	0.32/2.9	0.12/40	0.56/300	2.5K	Cubasch et al. 1992 [6]
τ_i	2.9	40	300		
α_i	0.2784			1.5K - 4.5K	Shine et al. 2005 [42]
τ_i	3.59×(climate sensitivity)				

†α: years^{-1}, τ: years

Table 4.2: Coefficients of Temperature Response Function

where the coefficients of the Shine et al. model are adjusted to the form of Equation 4.3 from a simple energy balance model. The Shine et al. model can apply different climate sensitivities to the temperature response function.

4.2.2 Non-CO_2 emission

The non-CO_2 effect of aviation emissions includes five different species, cirrus, sulfates, soot, water, and contrails, from fuel burn emission, and O_3 and CH_4 induced by NO_x emission. NO_x emission increases O_3 concentration in the short-term mode and decrease CH_4 concentration exponentially with a decay time of 11 years. The decreased CH_4 concentration results in the decreased O_3 concentration in the long-term mode, which has a same decay

Emissions	Reference RF† [mW/m^2]	Efficacy	Reference emissions index†
NO_x-O_3	21.9	1	$Q^{ref\,NO_x} = 21.6$ [Tg(NO_x)/yr]
H_2O	2.0	1	
Sulfate	-3.5	1	
Soot	2.5	1	$Q^{ref}_{fuel} = 169$ [Tg(fuel)/yr]
Contrails	10.0	1	
Cirrus	30.0	1	

† Sausen et al. 2005 [39]

Table 4.3: Short-lived RFs, efficacies, and emission indexes

time as CH_4, because CH_4 are one of ozone precursors. Non-CO_2 species except long-term O_3 and CH_4, which are represented as short-lived emissions in this thesis, are active in the atmosphere only during the emitted year, and long-term O_3 and CH_4 remain and decay with an exponential time constat of about 11 years. In contrast to the CO_2 impacts, RF of non-CO_2 emissions is calculated from fuel burn and NO_x emission inventories directly not from the concentration. The method of calculating temperature change from RF is same to the CO_2 case.

Radiative Forcing

Short-lived RF of the aviation emission is determined by scaling the normalized RF of CO_2 as shown in Equation 4.4 [40]. Table 4.3 summarizes the values related to the short-lived RF calculation.

$$RF^{*}_{short_i}(t) = \frac{\lambda_{short_i}}{\lambda_{CO_2}} \cdot \frac{RF^{ref}_{short_i}}{RF_{2xCO_2}} \cdot \frac{Q_{short_i}(t)}{Q^{ref}_{short_i}} \tag{4.4}$$

where

λ = sensitivity of the effect

$\lambda_{short_i}/\lambda_{CO_2}$ = efficacy of short-lived species i

RF^{ref}_{short} = reference RF of short-lived emission

RF_{2xCO_2} = 3.7 W/m^2 [24] (doubling CO_2 concentration)

$Q_{short}(t)$ = emitted mass of fuelburn or NO_x

Q^{ref}_{short} = reference emission index

For the NO_x induced impact of O_3 and CH_4, the reference RF is calculated from RF of short-lived O_3, $RF^{ref}_{O_3}$, scaled by the ratio of RF year values of CH_4 and short O_3 in Stevenson et al. 2004. [46]

$$RF^{ref}_{CH_4} = \frac{RFyr^{Stevenson}_{CH_4}}{RFyr^{Stevenson}_{short\ O_3}} \cdot \frac{RF^{ref}_{O_3} \cdot 1yr}{\tau_{CH_4}} \tag{4.5}$$

where $RFyr^{Stevenson}$ = integrated RF over 100 years

τ = 11.07 years (e-folding time)

The mean value of $RFyr^{Stevenson}_{CH_4}$ is -4.00 mW· yr/m^2, and the mean value of $RFyr^{Stevenson}_{short\ O_3}$ is 5.06 mW· yr/m^2. The reference RF of long-term O_3 is calculated in the same way of the reference RF of CH_4, and the mean value of $RFyr^{Stevenson}_{long\ O_3}$ is -0.92 mW· yr/m^2. The calculation of the normalized RF of CH_4 is shown in Equation 4.6. Calculating the normalized RF of CH_4 is similar to the calculation of the short-lived normalized RF, but the value is decayed exponentially during the lifetime of CH_4. It is same for the normalized RF of long-term O_3.

$$\begin{aligned} G_{CH_4}(t') &= RF^{ref}_{CH_4} \cdot e^{(-t'/\tau_{CH_4})} \\ RF^{*}_{CH_4}(t') &= \lambda_{CH_4} \int_{t_0}^{t'} \frac{Q_{NO_x}(t'')}{Q^{ref}_{NO_x}} \cdot \frac{G_{CH_4}(t'-t'')}{RF_{2xCO_2}} dt'' \\ &\approx \lambda_{CH_4} \sum_{n=0}^{N-1} \frac{Q_{NO_x}(t_0+n\Delta t)}{Q^{ref}_{NO_x}} \cdot \frac{G_{CH_4}(t'-t_0-n\Delta t)\cdot \Delta t}{RF_{2xCO_2}} \end{aligned} \tag{4.6}$$

where $N = (t' - t_0)/\Delta t$

4.3 Impact Valuation

4.3.1 Damage Function

The climate module uses the Nordhaus and Boyer (2000) damage function [36] to relate the temperature change to the economic cost. The damage function calculates a financial loss

as a percentage of GDP from a weighted sum of surface temperature change and squared surface temperature change, as shown in Equation 4.7.

$$D(t) = a_1 \Delta T_{1900}(t) + a_2 \Delta T_{1900}(t)^2 \tag{4.7}$$

where ΔT_{1900} is the temperature change since 1900, so $\Delta T_{1900}^{ref} = 0.6$ K [24] is added to the output temperature change of the climate module to adjust the temperature change since 1900. The coefficients of the damage function are -0.0045 for a_1 and 0.0035 for a_2 for calculating the global impact. Since the Nordhaus and Boyer damage function includes a non-linear term, the squared temperature change, the individual impact of emissions cannot be calculated independently but should be considered with respect to the anthropogenic effect and other emissions effects. The climate module calculates the effect of one emission species by subtracting the effect of all anthropogenic emissions except the considered emission from the all anthropogenic emission effect.

The cost in dollars is also calculated by multiplying the projected GDP values to the damage result in the metric of % GDP. The GDP projection is based on the quadratic extrapolation of matched IS92 scenarios. Figure 4-4 shows the GDP projection according to the IS92 scenarios.

$$r(t) = \frac{\mu}{1 + t\sigma^2/\mu} \tag{4.8}$$

4.3.2 Net Present Value of Climate Impact

The Net Present Value (NPV) of the cost caused by temperature change is another metric of the climate impact valuation. The climate module calculates the present value of future effects of aviation emissions by discounting the cost with discount rate. NPV is the sum of this discounted cost. There are several suggestion of future discount rate.

$$value(t) = \frac{value(t + n\Delta t)}{(1 + r)^n} \tag{4.9}$$

where r = discount rate

$\Delta t = 1$ year for yearly discounting

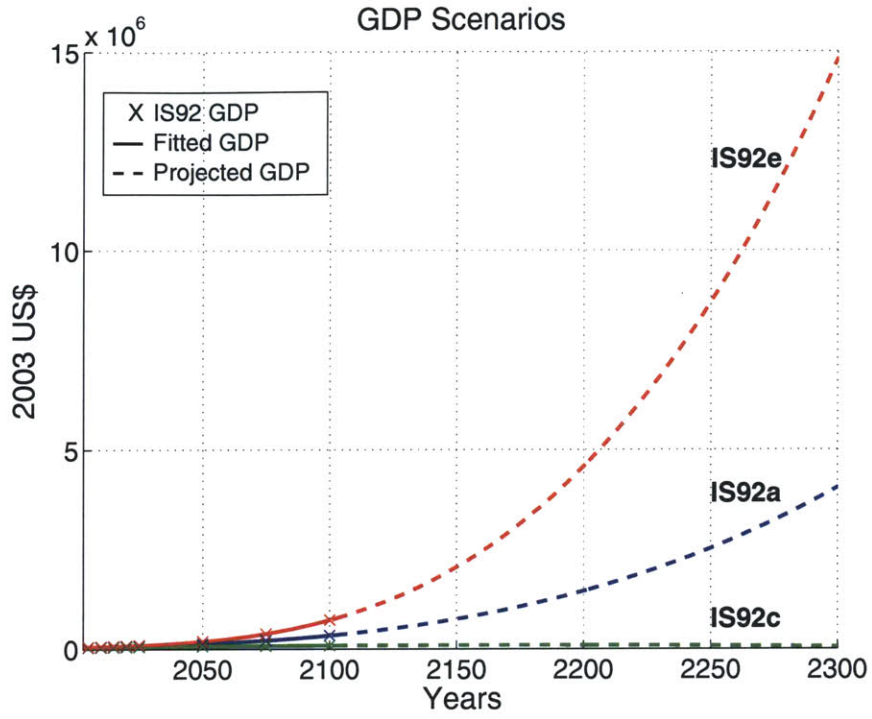

Figure 4-4: GDP projection for IS92 Scenarios

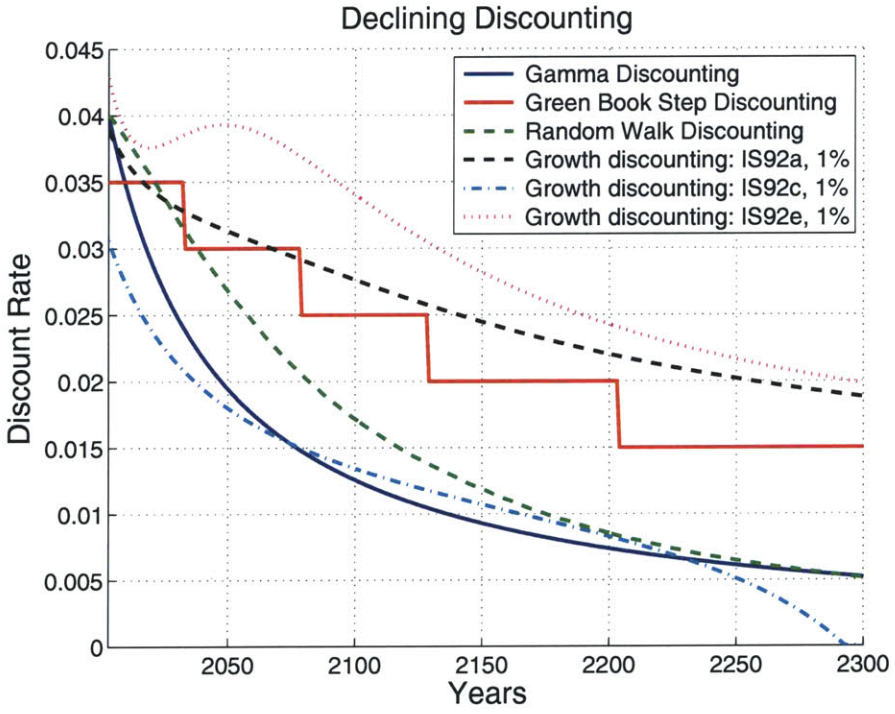

Figure 4-5: Declining discount rate approaches

Period [yeras]	Discount rate (%)
0-30	3.5
31-75	3.0
76-125	2.5
126-200	2.0
201-300	1.5
301+	1.0

Table 4.4: Recommended future discount rate of UK GreenBook

The simplest discounting scheme is a constant discount rate during entire impact years, which can be calculated easily with Equation 4.9. However, the constant discounting may underestimates the benefits of long-lived GHGs mitigation efforts [35]. Another approach is the declining discount rate across impact years. Figure 4-5 shows four suggestions of declining discounting: Green book discounting [20], Gamma discounting [48], Random walk discounting [34], and Growth discounting [15]. These declining discounting approaches consider the uncertainty in the future. Weitzman's gamma discounting in Equation 4.8 is based on the assumption that the future discount rate follows a gamma distribution, and the parameters deciding the shape of the gamma distribution were found from a questionnaire of economists, where the findings are $\mu = 0.04$ and $\sigma = 0.03$. UK Green Book (2003) also presents a recommendation of social discount rate for a policy making. The recommended values are shown in Table 4.4. Random walk discounting reflects a random movement of discount rate inside lower and higher envelopes of a possible discount rate range based on the past data [35]. The resulting discount rate is declining because the effective discount rate is closer to the lower envelope if discount rate is randomly drawn inside the range. The growth rate discounting is based on the Social Time Preference Rate (STPR) in Equation 4.10. It is suggested ρ is between 1% and 1.6% and μ is around 1 [20].

$$r = \rho + \mu \cot g \tag{4.10}$$

where

$r = STPR$

$\rho =$ pure rate of time preference

$\mu =$ elasticity of the marginal utility

$g =$ growth rate of per capita consumption

4.4 Output Results

Figures in this section are examples of the graphical presentation of outputs in the climate module. Figure 4-6 shows the surface temperature change and Figure 4-7 shows the damage in terms of % GDP when the aviation emissions are emitted as a one year impulse. The single year is simulated based on the AEDT/SAGE 2003 data during 800 impact years. Figures only show the calculation result during first 300 years. The plots of the impulse aviation emission provide information about the behavior of GHGs after being emitted. While the effects of short-lived emissions diminish rapidly, the CO_2 effect increases after the end of emissions and remains at the atmosphere long time. In the damage metric, emission effects remain longer and disappear more slowly than in the temperature change, and as a result, the CO_2 effect becomes more significant in the damage result. Figure 4-8 and Figure 4-9 show the temperature change and the damage result of scenario aviation emission with Fa1 up to 2100. Impact was calculated during 800 years after the end of emission in 2100. The result plots of the scenario emission show the GHGs' effects during emission, where the effects of short-lived emissions are also important as well as CO_2.

4.5 Uncertainty Assessment

Table 4.5 shows assumptions and inputs in the climate module. Scientific uncertainties in input variables, such as climate sensitivity and short-lived RF values, are regarded as having best estimation values or ranges and are presented as probabilistic distributions in the uncertainty assessment. Most of the uncertainty assessment focuses on these kinds of uncertainties. Assumptions, such as the emission scenario and discount rate, are treated as a user's choice rather than distributions. The impact of this type of uncertainty can be assessed with the local sensitivity analysis. All uncertainty assessments in the climate module are based on Monte Carlo simulations with probabilistic distributions. Instead of the NRSA with all fixed values, a composite method of the sensitivity analysis and the Monte Carlo simulations, called as the hybrid Monte Carlo (HMC) sensitivity analysis in this thesis, is suggested to capture the uncertainty in the assumption choices, which are not applicable to be represented as a distribution, while retaining the uncertainty in other input variables. For the sensitivity analysis and the VABO Monte Carlo analysis, baseline values are defined for each of the assumptions and inputs as shown in Table 4.5. The baseline uses

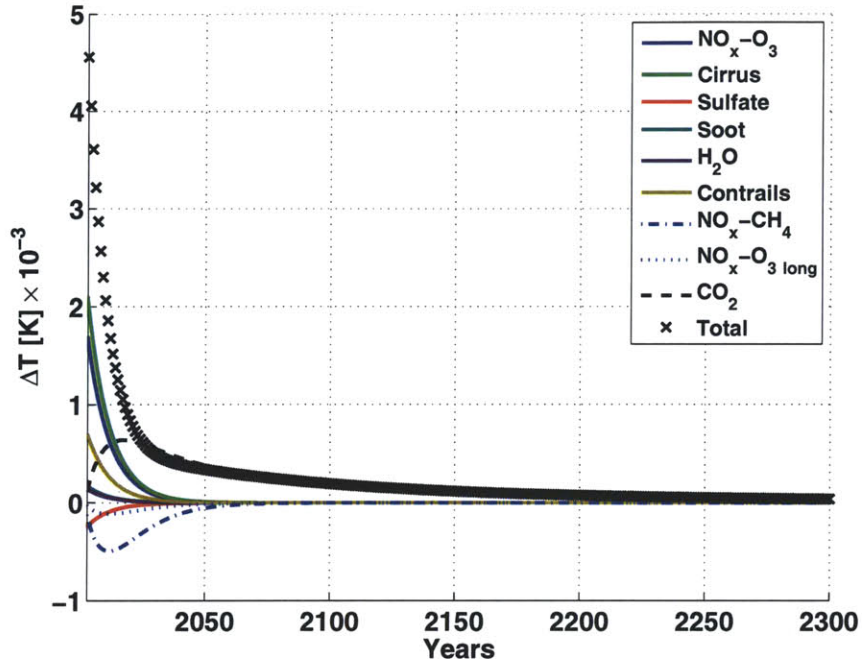

Figure 4-6: Temperature change caused by SAGE impulse aviation emission

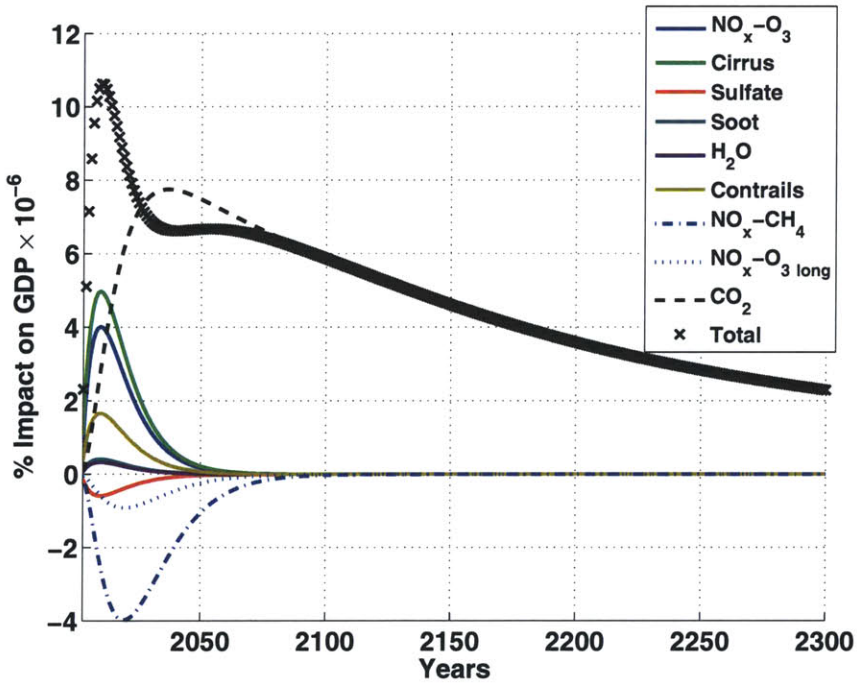

Figure 4-7: Damage caused by SAGE impulse aviation emission

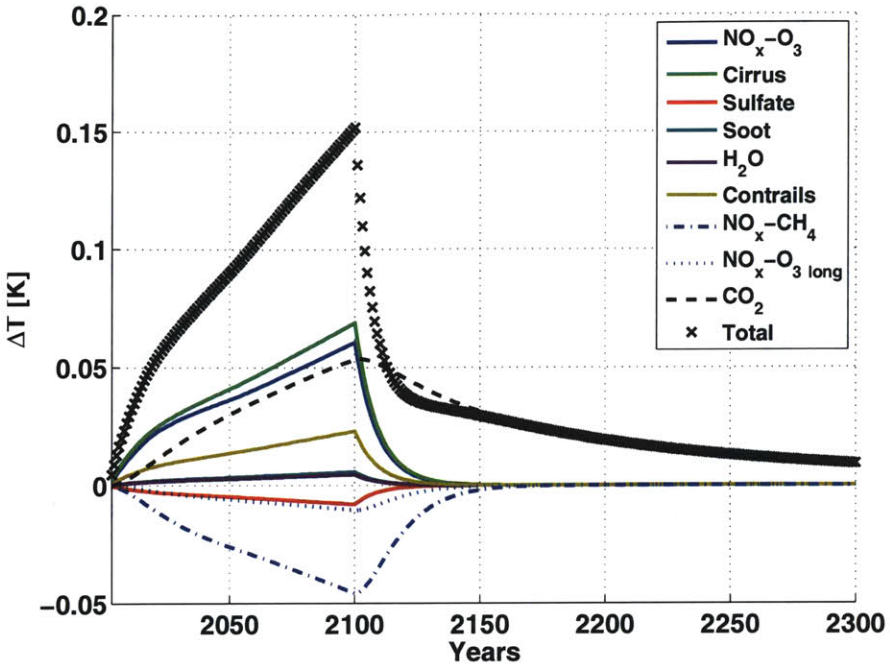

Figure 4-8: Temperature change caused by Fa1 scenario aviation emission

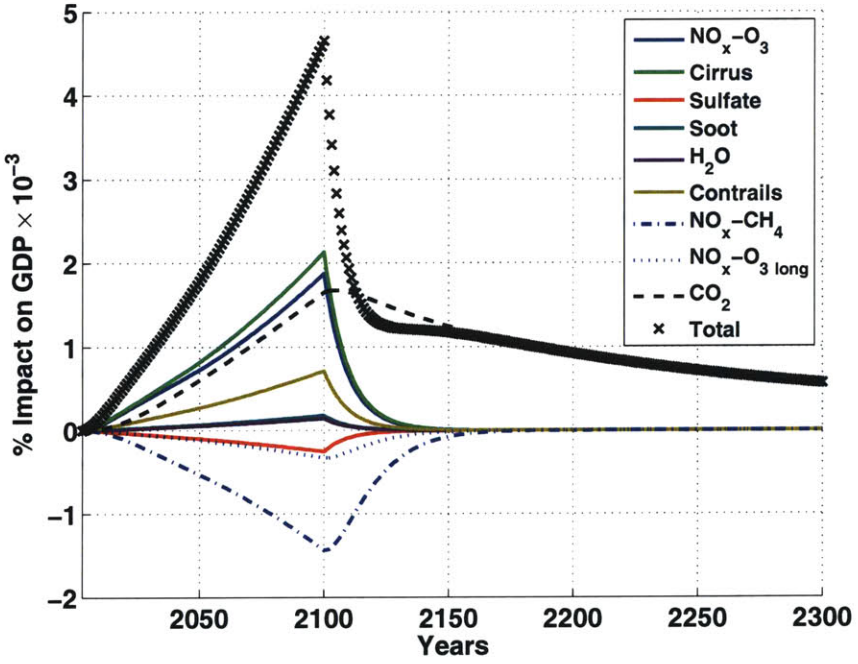

Figure 4-9: Damage caused by Fa1 scenario aviation emission

Assumptions	Baseline Values
Anthropogenic emissions	IS92a
Aviation emissions	Fa1
Carbon cycle model	Bern carbon cycle
Temperature response model	Shine et al.
Discount rate	3.5%
Inputs	**Baseline Values**
Climate sensitivity	2.5K
RF doubling CO_2	3.7 W/m^2
RF* short-lived	[21.9 (NO_x-O_3); 2 (H_2O); -3.5 (sulfate); 2.5 (soot); 10 (contrails); 30 (cirrus)] mW/m^2
Short-lived efficacy	all set to 1
e-folding time (CH_4 & long-term O_3)	11.07 years
RF-yr CH_4	-4.00 mW· yr/m^2
RF-yr long-term O_3	-0.92 mW· yr/m^2
RF-yr short-term O_3	5.06 mW· yr/m^2
Reference temperature change 1900	0.6K

Table 4.5: Assumptions and inputs of the climate module and their baseline values

the IS92-Fa1 emission scenario; the Bern model for the carbon cycle model; Shine et al. model with 2.5K climate sensitivity for the temperature response model; 3.7 W/m^2 for RF of doubling CO_2; short-lived RF values from Sausen et al. 2005 [39]; short-lived emissions efficacies set to all 1; mean values of Stevenson et al. 2004 [46] for e-folding time and RF-yr values of CH_4 and long-term O_3; 0.6K for the reference temperature chance since 1900 for the damage function; and 3.5% discount rate.

4.5.1 Input Distributions

This section describes the probabilistic distributions of input variables for the Monte Carlo simulations. The uniform distribution is used for the input variables where a best estimate is not available such as the emission increment, climate sensitivity, and efficacy; and the triangular distribution is used for the input variables whose best estimate is available like RF for short-lived effects and doubling CO_2. Table 4.6 shows the input variables and their distribution types and ranges.

The best estimate of RF's for short-lived effects are based on the values of Sausen et al.,2005 [39], and upper and lower limits of RF for short-lived effects are based on the

Input Variables	Description	Distribution[§]
Reference Temperature Change	Reference temperature change in damage function from IPCC TAR	Triangular [0.4K; 0.6K; 0.8K]
RF doubling of CO_2	Based in IPCC TAR	Triangular [3.5; 3.7; 4.2] W/m^2
RF short-lived effects	Radiative forcing for [NO_x-O_3; NO_x-CH_4; H_2O; sulfate; soot; contrails; cirrus]	Triangular [0, 21.9, 35; N/A; 0, 2, 6; -7.5, -3.5, 0; 0, 2.5, 5; 0, 10, 30; 0, 30, 80] mW/m^2
Efficacies for short-lived effects	Distribution between all set to 1 and values of Hansen et al. (2005) [16]	Uniform [0.82, 1; 1, 1; 1, 1.09; 0.78, 1; 1, 1; 0.59, 1]
Emission increment (fuelburn, CO_2)	Uncertainties in emissions inventories	Uniform [-5%, +5%]
Emission increment (NO_x)	Uncertainties in emission inventories	Uniform [-10%, +10%]
e-folding time & $RFyr_{CH_4}$ & $RFyr_{short\ O_3}$	Month values from Stevenson et al. (2004)	Discrete between [Jan, 11.13, -3.83, 4.51], [Apr, 11.05, -4.00, 5.30], [Jul, 11.09, -4.42, 5.14], [Oct, 10.99, -3.76, 5.17], where [month, e-folding time (years), $RFyr_{CH_4}$ ($mW/m^2 \cdot yr$), $RFyr_{short\ O_3}$ ($mW/m^2 \cdot yr$)]
e-folding time & $RFyr_{long\ O_3}$ & $RFyr_{short\ O_3}$	Month values from Stevenson et al. (2004)	Discrete between [Jan, 11.13, -0.90, 4.51], [Apr, 11.05, -0.89, 5.30], [Jul, 11.09, -0.99, 5.14], [Oct, 10.99, -0.89, 5.17], where [month, e-folding time (years), $RFyr_{long\ O_3}$ ($mW/m^2 \cdot yr$), $RFyr_{short\ O_3}$ ($mW/m^2 \cdot yr$)]
Climate sensitivity	Based on IPCC TAR	Uniform [1.5K; 4.5K]

[§] Triangular distribution: [lower limit; mode; upper limit]

Uniform distribution: [lower limit; upper limit]

Table 4.6: Input Distributions for Monte-Carlo Simulation

adjusted IPCC TAR limits with expert opinions. The e-folding time, RF-yr values of CH_4 or long-term O_3, and RF-yr values of short-term O_3 are grouped as 4 possible pairs rather than presented as continuous distributions because RF values are associated with monthly emission perturbations in Stevenson et al. [46]. A discrete distribution is used to choose one pair.

4.5.2 Convergence Error

Uncertainty assessments of the climate module focus on the identification of contributions to the variability in the response variable to input variables. Since output variables are not normally distributed, the non-parametric bootstrap technique was used to estimate the 95% confidence interval of mean and variance. The bootstrap technique is a numerical re-sampling method for estimating statistical inference. A bootstrap sample is randomly drawn as a same size to the original data with replacement from the original observed data. The statistics, such as mean, variance, or confidence intervals, are evaluated with Monte Carlo simulations to draw a large number of bootstrap samples. 50 to 200 of bootstrap samples are enough for most cases [10]. The bootstrap technique does not require an assumption about underlying distributions like a normal distribution because the bootstrap is based on re-sampling from the observed data not a probabilistic distribution function. The criterion of convergence error is shown in Equation 4.11.

$$\text{Convergence error} = \frac{\text{[variance or mean] of output} - \text{lower ci}}{\text{[variance or mean] of output}} \tag{4.11}$$

For the VABO Monte Carlo analysis, the convergence error is 2.1% for the mean shift and 5.0% for the variance shift with 3000 iterations of Monte Carlo simulation. For global sensitivity analysis, the convergence error is 2.5% for the variance shift with 10000 iterations of Monte-Carlo simulation. The number of iteration increased in the global sensitivity simulation because of its slow convergence rate. Figure 4-10 and Figure 4-11 shows the convergence history of global sensitivity simulations. The normalized approach for the Sobol's index and the normalized alternative approach for the total sensitivity analysis are most stable and converge fastest. Therefore, the normalized approach and normalized alternative approach were used for calculating the Sobol's index and the total sensitivity as was the case with the aircraft price model assessment.

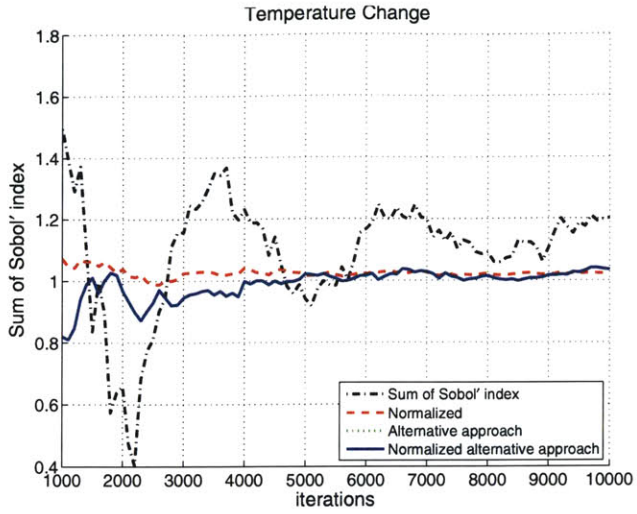

(a) Temperature Change

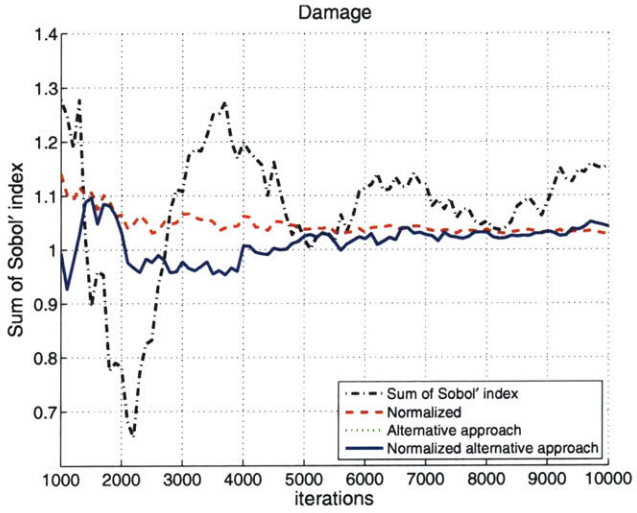

(b) Damage

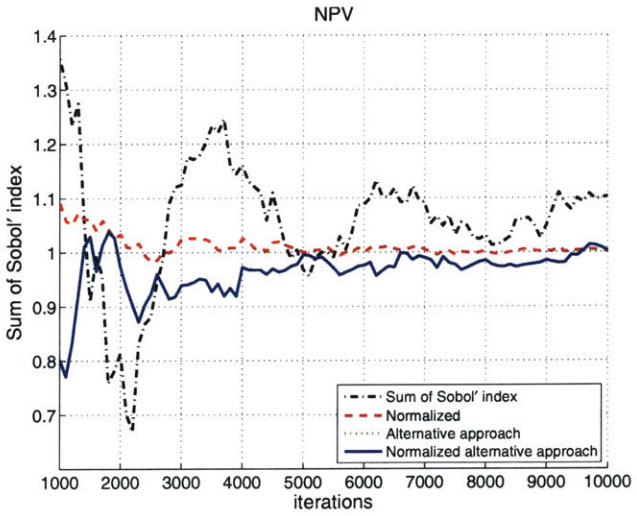

(c) Net Present Value

Figure 4-10: Convergence history of sum of Sobol's indices

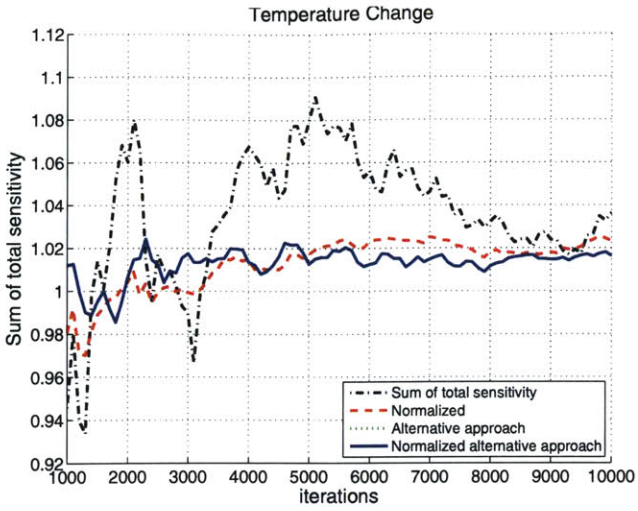

(a) Temperature Change

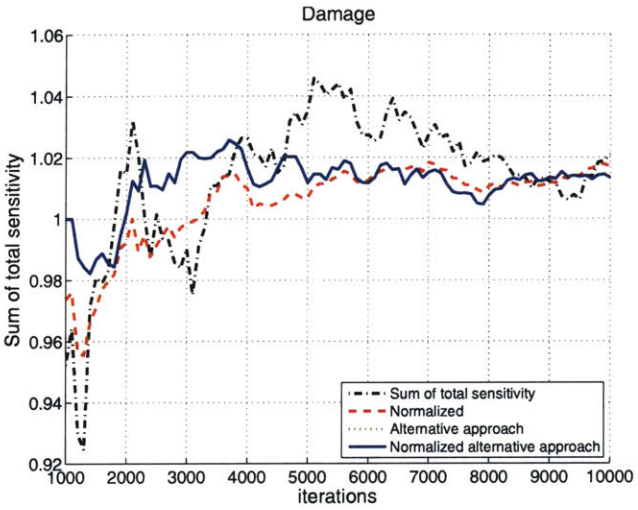

(b) Damage

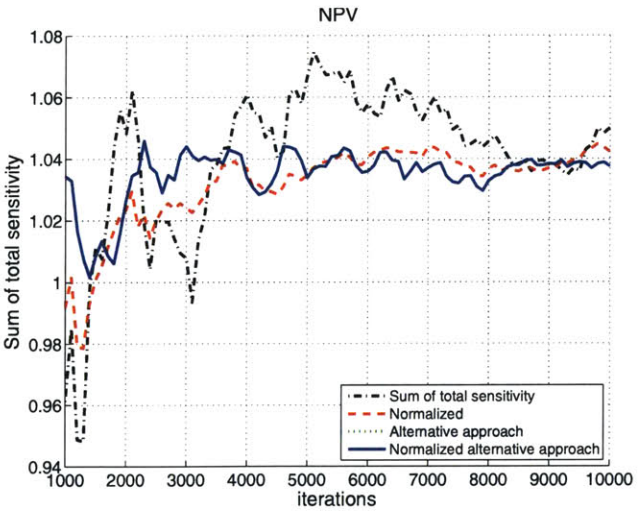

(c) Net Present Value

Figure 4-11: Convergence history of sum of total sensitivities

4.5.3 Monte Carlo Regression Analysis

Table 4.7 shows the standardized regression coefficients of the first order regression model with input variables where 3000 randomly drawn samples were used. The insignificant coefficients are presented as "ns". The contributions to the variance were calculated from the squared standard betas. RF of clouds and the climate sensitivity are most significant variability sources. Except for the RFs of clouds and contrails, RF of doubling CO_2, and the climate sensitivity, it is not meaningful to rank the contributions to the variance because the effects are very small. The result also shows that the contribution of short-lived effects decreases in the damage result while the contributions of RF for doubling CO_2 and the climate sensitivity increase in the damage. The decreased contribution of short-lived effects is caused by the increased CO_2 effect with a long impact time. The contribution of short-lived effects increases again in the NPV because short-lived effects in near future are less discounted relative to the CO_2 effect in the long future.

4.5.4 Vary-all-but-one Monte Carlo Analysis

Table 4.8 shows the result of the VABO Monte Carlo analysis. The variable name in the case column indicates the Monte Carlo simulation with all varying except that variable. The VABO Monte Carlo simulation result was compared to the full Monte-Carlo simulation result to identify the mean shift and the variance shift. The mean shift shows how much the variable affects the mean bias of the output variables, and the variance shift shows the contribution of input variables to the variability in the outputs. Significant results larger than the convergence error, 2.1% for the mean shift and 5.0% for the variance shift, have an asterisk next to the number.

Mean biases are more severe in the damage and NPV, at 43% and 42% each, than in the temperature change at 24%, because the output distributions become more skewed in the damage and NPV. The major contribution to skewness comes from climate sensitivity as shown in Figure 4-12. Also, the contribution to the variance of climate sensitivity is the most significant and the contribution of short-lived RF is next, and climate sensitivity and short-lived RF contribute to the mean bias significantly. Figure 4-12 shows that higher climate sensitivity results in the greater mean responses and the variance in outputs. The effect of the uncertainty in short-lived RF relatively decreased in the damage than in the

temperature change because the effect of CO_2 becomes more important in the damage as shown in Figure 4-8 and 4-9. However, the effect of CO_2 decreases in NPV relative to in the damage because the CO_2 impact in the distant future is discounted.

Case	Integrated Temperature Change		Integrated Damage Estimate		NPV estimate (3.5% Discount rate)	
	Std. Beta	Contribution to var.	Std. Beta	Contribution to var.	Std. Beta	Contribution to var.
ΔT^{ref}_{1900}	-	-	0.017	0.0%	0.030	0.1%
RF_{2xCO_2}	0.063	0.4%	0.117	1.4%	0.093	1.0%
RF^* short-lived						
NO_x-O_3	-0.031	0.1%	-0.025	0.1%	-0.015	0.0%
clouds	0.435	20.2%	0.186	3.7%	0.370	15.1%
sulfate	0.055	0.3%	0.022	0.1%	0.046	0.2%
soot	0.050	0.3%	0.018	0.0%	0.042	0.2%
H_2O	0.036	0.1%	0.012	0.0%	0.030	0.1%
contrails	0.127	1.7%	0.053	0.3%	0.106	1.2%
Short-lived efficacy						
NO_x-O_3	0.028	0.1%	0.010	0.0%	0.022	0.1%
clouds	-	-	-	-	-	-
sulfate	ns	ns	ns	ns	ns	ns
soot	0.006	0.0%	ns	ns	ns	ns
H_2O	-	-	-	-	-	-
contrails	0.038	0.2%	0.016	0.0%	0.030	0.1%
Emission increment (fuelburn, CO_2)	0.086	0.8%	0.051	0.3%	0.052	0.3%
Emission increment (NO_x)	ns	ns	ns	ns	ns	ns
e-folding time & $RFyr_{CH_4}$ & $RFyr_{short\ O_3}$ †	0.040	0.2%	0.021	0.0%	0.032	0.1%
e-folding time & $RFyr_{long\ O_3}$ & $RFyr_{short O_3}$ †	0.008	0.0%	ns	ns	ns	ns
Climate sensitivity	0.842	75.6%	0.942	94.0%	0.859	81.5%

† e-folding time, $RFyr_{CH_4}$ ($RFyr_{long\ O_3}$), $RFyr_{short\ O_3}$ were chosen as a group with discrete distribution.

Table 4.7: Result of Monte Carlo regression analysis

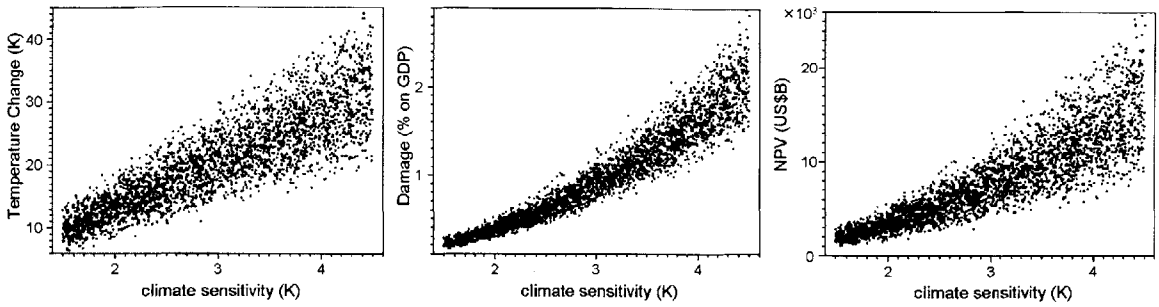

(a) Temperature Change (b) Damage (c) Net Present Value

Figure 4-12: The relationship between climate sensitivity and output responses

	Integrated Temperature Change [K·yr]		Integrated Damage Estimate [%GDP·yr]		NPV estimate (3.5% Discount rate) [2003US$ $\times 10^9$]	
Case	Mean	Variance	Mean	Variance	Mean	Variance
All varying	21	53	0.98	0.32	8000	22100
Case	% shift‡ of Mean	Variance	% shift‡ of Mean	Variance	% shift‡ of Mean	Variance
Deterministic§	-23.8%	-	-43.2%	-	-42.0%	-
ΔT_{1900}^{ref}	-	-	-0.4%	-3.8%	-0.7%	-8.6%*
RF_{2xCO_2}	-0.2%	-6.6%*	-4.4%*	-11.8%*	-4.1%*	-11.8%*
RF* short-lived	-10.4%*	-37.3%*	-7.5%*	-14.7%*	-14.7%*	-39.7%*
Short-lived efficacy	3.1%*	1.9%	1.2%	3.7%	3.9%*	4.8%
Emission increment (fuelburn, CO_2)	-0.7%	-2.1%	-0.6%	-0.6%	-1.0%	-2.6%
Emission increment (NO_x)	-1.6%	-2.9%	-1.7%	0.0%	-2.5%*	-4.9%
e-folding time & $RFyr_{CH_4}$ & $RFyr_{short\ O_3}$†	-1.5%	-5.8%*	-1.9%	-4.3%	-2.6%*	-7.1%*
e-folding time & $RFyr_{long\ O_3}$ & $RFyr_{short\ O_3}$†	-1.2%	-3.7%	-1.3%	-0.0%	-1.8%	-3.7%
Climate sensitivity	-18.0%*	-84.9%*	-38.1%*	-97.8%*	-34.5%*	-92.8%*

§ Baseline case for all inputs

† e-folding time, $RFyr_{CH_4}$ (or $RFyr_{long\ O_3}$), and $RFyr_{short\ O_3}$ were chosen as a group with a discrete distribution.

‡ % Mean and variance shift are relative to case of all varying.

Table 4.8: Result of Vary-all-but-one Monte Carlo analysis

4.5.5 Hybrid Monte Carlo Sensitivity

This section provides a sensitivity analysis of important input variables and assumptions with their nominal ranges. For the sensitivity analysis of important input variables, three input variables, short-lived RF, short-lived efficacy, and climate sensitivity were chosen based on the result of VABO Monte Carlo analysis. The hybrid Monte Carlo (HMC) simulation varies the selected three parameters deterministically to their nominal range while other input variables are randomly drawn from the probabilistic distributions of the full-varying Monte Carlo simulation. One parameter is varied at a time and the other parameters are fixed at their baseline values. For the sensitivity analysis of assumptions, four assumptions in Table 4.5 were investigated with their available options where the scenarios of anthropogenic emission are varied with matched aviation emission scenarios together. When investigating the sensitivity to assumptions, three selected input variables are fixed at their baseline values and other input variables are randomly drawn from the defined distributions. The baseline values, nominal range, and available choices of input variables and assumptions used in the HMC simulation are summarized in Table 4.9.

The HMC sensitivity analysis allows the comparison of the effect of input variable uncertainty with the effect of assumption choices. It also allows investigation of the biased direction of the input variable distributions as well as the magnitude of contributions to variance. The HMC analysis result in Table 4.10 shows RF* short-lived and climate sensitivity contribute to mean and standard deviation shift significantly compared to short-lived efficacy. Also, the contribution of climate sensitivity is increased in the damage and NPV especially with high climate sensitivity. In the aviation scenario choice, the estimates of temperature change and damage are lowest with the IS92a-Fa1 scenario, but NPV estimation is lowest with the IS92c-Fc1 scenario. This non-constant trend in the scenario choice sensitivity comes from the fraction of CO_2 and non-CO_2 effects and the discount rate effect. Figure 4-13 illustrates the contributions of each emission to outputs. The CO_2 effect is largest with the IS92c-Fc1 scenario, lowest with the IS92e-Fe1, and not much different between IS92a-Fa1 and IS92e-Fe1 in the temperature change. Although aviation CO_2 emission is lowest in the Fc1 scenario, the temperature change caused by CO_2 emission is largest in the IS92c-Fc1 scenario because the logarithmic relationship between RF and the emission concentration. While the increment of RF by CO_2 emission is small in the high

Assumptions	Baseline values	Other options
Aviation emission & anthropogenic emission	IS92a-Fa1	IS92c-Fc1, IS92e-Fe1
Carbon cycle model	Bern carbon cycle	†Hooss et al. 2001, Hasselmann et al. 1993, Hasselmann et al. 1997
Temperature response model	Shine et al.	‡Hooss et al. 2001, Hasselmann et al. 1993 (1 mode), Hasselmann et al. 1997 (3 mode LSG§), Cubasch et al. 1992 (3 mode CGCM*)
Discount rate	3.5%	0%, 1%, 5%
Inputs	**Baseline values**	**Nominal range**
Climate sensitivity	2.5K	1.5K - 4.5K
RF* short-lived [NO_x-O_3; H_2O; sulfate; soot; contrails; cirrus]	[21.9; 2 ; -3.5; 2.5; 10; 30] mW/m^2	[0; 0; 0; 0; 0; 0] - [35; 6; -7.5; 5; 30;80]
Short-lived efficacy	all set to 1	The values in Hanson et al. [16]: [0.82; 1; 1.09; 0.78; 0.59; 1]

† See Table 4.1, ‡ See Table 4.2

§ The Large Scale Geostrophic ocean model

* The Coupled ocean-atmosphere General Circulation Model

Table 4.9: The description of parameters in the Hybrid Monte Carlo sensitivity analysis

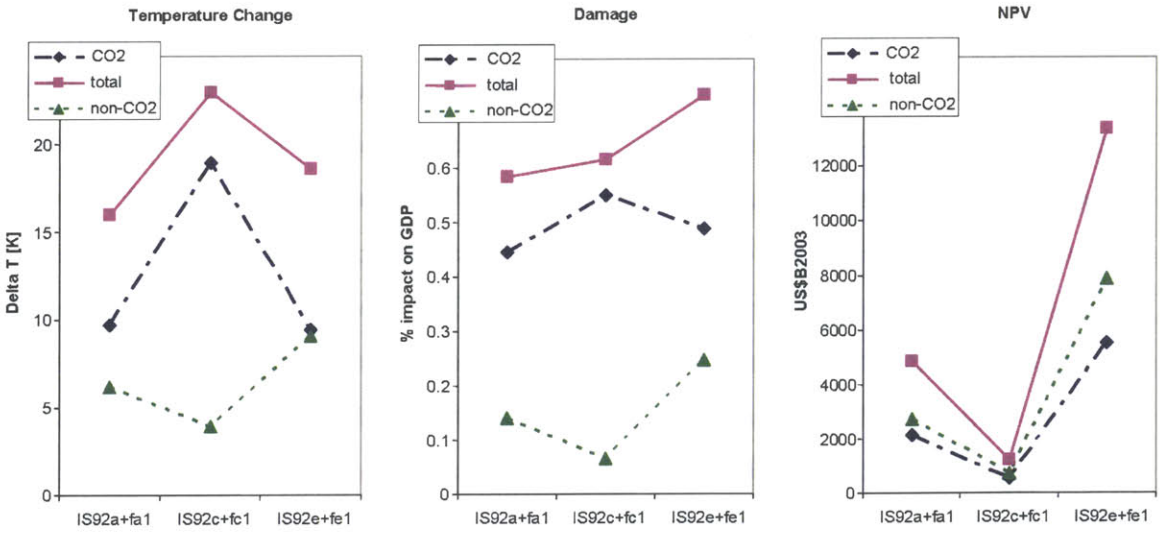

Figure 4-13: Contribution to outputs of CO_2 and non-CO_2 emissions

background CO_2 concentration and large in the low background CO_2 concentration, the Non-CO_2 effect is proportional to the amount of emission. As a result, the temperature change from the non-CO_2 effect is largest in the IS92e-Fe1 scenario and lowest in the IS92c-Fc1 scenario. The complement between CO_2 and non-CO_2 effects makes the lowest total temperature change in the IS92a-Fa1 scenario. In the damage, the relative CO_2 effect becomes greater than the non-CO_2 effect compared to the temperature change, but the slowly diminished and accumulated CO_2 damage decreases the difference of CO_2 effects between scenarios. While the CO_2 effect in the IS92e-Fe1 scenario is smaller than the CO_2 effect in the IS92c-Fc1 scenario, the total damage estimation is largest in the IS92e-Fe1 scenario because of the largest non-CO_2 effect. When looking at the NPV estimation, the discount rate effect makes entirely different result. The CO_2 effect in the distant future is discounted excessively compared to the non-CO_2 effect whose contribution is significant in the near future mainly, and as a result, the CO_2 effect becomes less than the non-CO_2 effect. Also, the CO_2 effect in the IS92c-Fc1 scenario is discounted more compared to the CO_2 effect in IS92e-Fc1 because the decreasing background CO_2 emission scenario of IS92c-Fc1 generates a large amount of the CO_2 effect in the distant future relatively. With the highest CO_2 and non-CO_2 effect, the total NPV estimation is greatest in the IS92e-Fe1 scenario.

Impacts of the carbon cycle model and the temperature response model were also investigated. Figure 4-15 and Figure 4-16 show the temperature change and the damage of different carbon cycle models and temperature response models over impact years. As shown in Figure 4-15, the impact of each carbon cycle model to the temperature change is not much different across all impact years. The model in Hooss et al. (2001) gives a very similar result to the Bern CC model. The difference of impacts in the temperature response models is larger than the difference in the carbon cycle models. The simple energy balance model in Shine et al. (2005) overestimates the climate impacts in the emission stage compared to the LSG model and the CGCM in Hasselmann et al. (2007). The 1 mode model of Hasselmann et al. (1997) does not present well the diminished emission effect after the end of emission.

The sensitivity result of discount rate shows that the discount rate choice has a very significant influence on result. If the discount rate choice is changed to 1% from 3% of the baseline, the mean and standard deviation of the NPV estimation increases about 1520% and 1750% each. This mean bias and the variance increment become excessive as discount

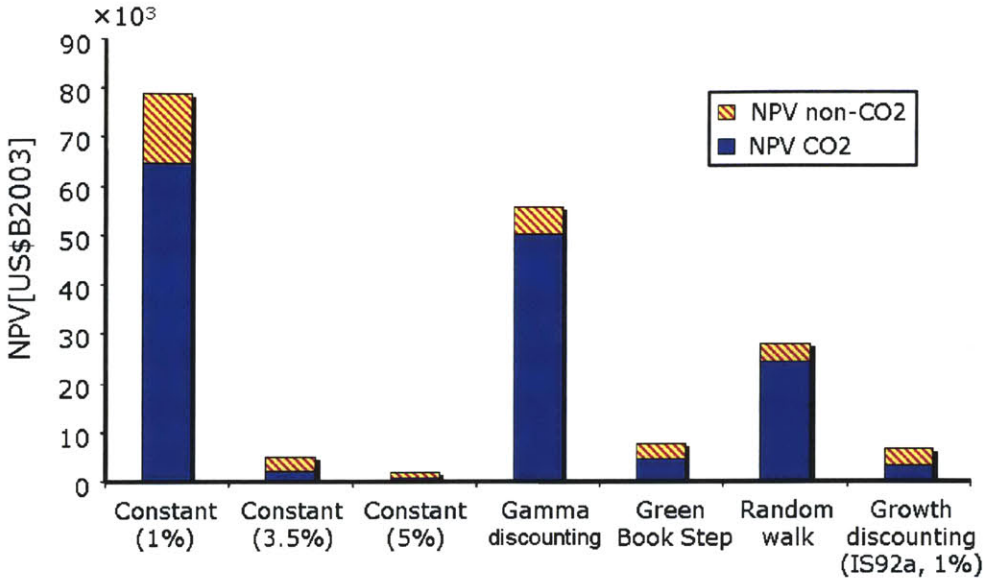

Figure 4-14: NPV estimation with various discount rate choices

rate decreases. Figure 4-14 shows additional sensitivity analysis results with several discount rate options that appeared in Section 4.3.2. The NPV estimation for 3.5% constant discount rate is similar to the estimation with the Green Book Step discount rate approach and the growth discounting approach with 1% of ρ in Equation 4.10 and the growth rate calculated from the IS92a GDP scenario, but the fraction of CO_2 effect in NPV is higher in the Green Book discounting and growth rate discounting. The cost of CO_2 emission is estimated more highly with declining discounting than with constant discounting.

4.5.6 Global Sensitivity

Table 4.11 shows the result of Sobol's index and total sensitivity. Significant results larger than the convergence error, 2.5%, have an asterisk next to the number. The main effects of climate sensitivity and short-lived RF contribute to the variability in outputs significantly, and the contributions of other input variables are insignificant. The significant variables are not changed when considering the interaction effect in the total sensitivity. This suggests that there are no significant interactions related to the variables except the climate sensitivity and short-lived RF. It is notable that the total sensitivity numbers are very similar to the contribution to variance in the MC regression result. Results in the total sensitivity are a little larger than the result in MC analysis, and the difference becomes larger in the NPV where the assumption of a first order model is not adequate.

	Integrated Temperature Change [K·yr]		Integrated Damage Estimate [%GDP·yr]		NPV Estimate [2003US$ $\times 10^9$]	
Case	Mean	Std dev.	Mean	Std dev.	Mean	Std dev.
Baseline[§]	16	0.64	0.58	0.04	4842	343

Case		% shift[‡]		% shift[‡]		% shift[‡]	
		Mean	Std dev.	Mean	Std dev.	Mean	Std dev.
Discount rate	0%	-	-	-	-	89100%	105000%
	1%	-	-	-	-	1520%	1750%
	5%	-	-	-	-	-62%	-63%
RF* short-lived[†]	lower	-39%	-26%	-24%	-16%	-57%	-46%
	upper	71%	65%	47%	38%	106%	94%
Short-lived efficacy	Hanson et al., 2005	-9%	-2%	-6%	-4%	-12%	-8%
Climate sensitivity	1.5K	-42%	-42%	-67%	-66%	-65%	-61%
	4.5K	84%	84%	239%	233%	200%	185%
Aviation Scenario*	Fc1	44%	58%	5%	14%	-74%	-72%
	Fe1	16%	17%	26%	23%	176%	174%
Carbon Cycle Model	Hooss 2001	-3%	-4%	-4%	-6%	8%	5%
	Hasselmann 1993	-14%	-15%	-36%	-36%	-32%	-30%
	Hasselmann 1997	-12%	-13%	-32%	-32%	-26%	-24%
Temperature Response Model	Hooss 2001	-9%	-19%	-15%	-59%	-52%	-62%
	Hasselmann 1 mode	1%	-8%	1%	-52%	-38%	-55%
	Hasselmann 3 mode LSG	-30%	-37%	-52%	-75%	-68%	-72%
	Hasselmann 3 mode CGCM	-8%	-18%	-12%	-57%	-75%	-77%

[§] Baseline cases: discount rate = 3.5%, RF* short-lived = reference values from Sausen et al. 2005 [39], short-lived efficacies = all set to 1, climate sensitivity = 2.5K, aviation scenario = IS92a-Fa1, carbon cycle model = Bern CC, temperature response model = Shine

[†] Lower and upper bounds of short-lived RF* are based on IPCC TAR limits in Table 4.9

* Matched background emission scenarios are used. (IS92a-Fa1, IS92c-Fc1, IS92e-Fe1)

[‡] % shifts are relative to baseline case.

Table 4.10: Result of Hybrid Monte Carlo sensitivity analysis

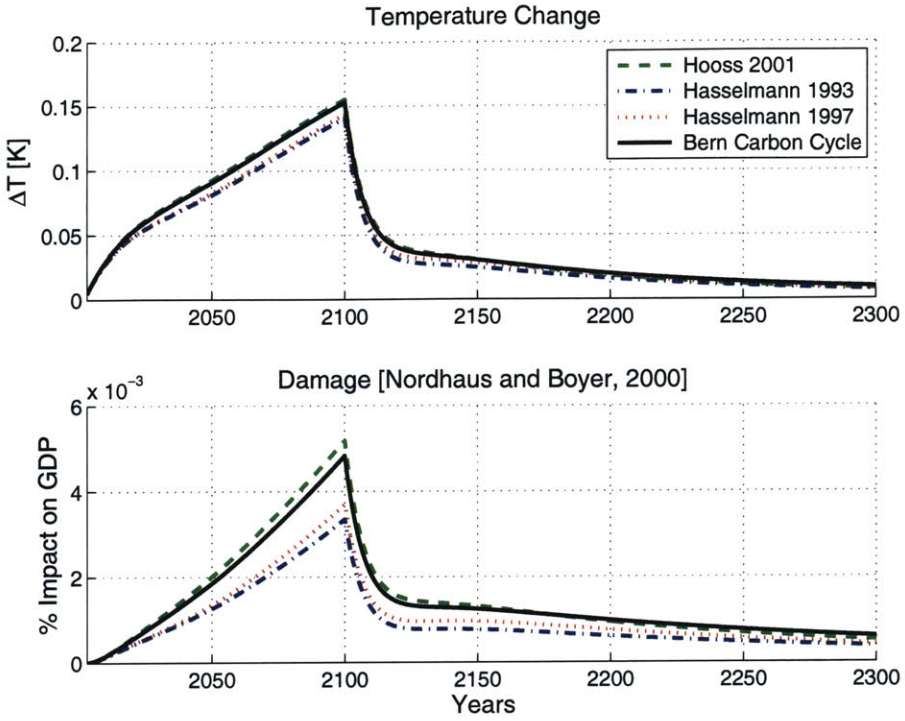

Figure 4-15: Impact of carbon cycle model

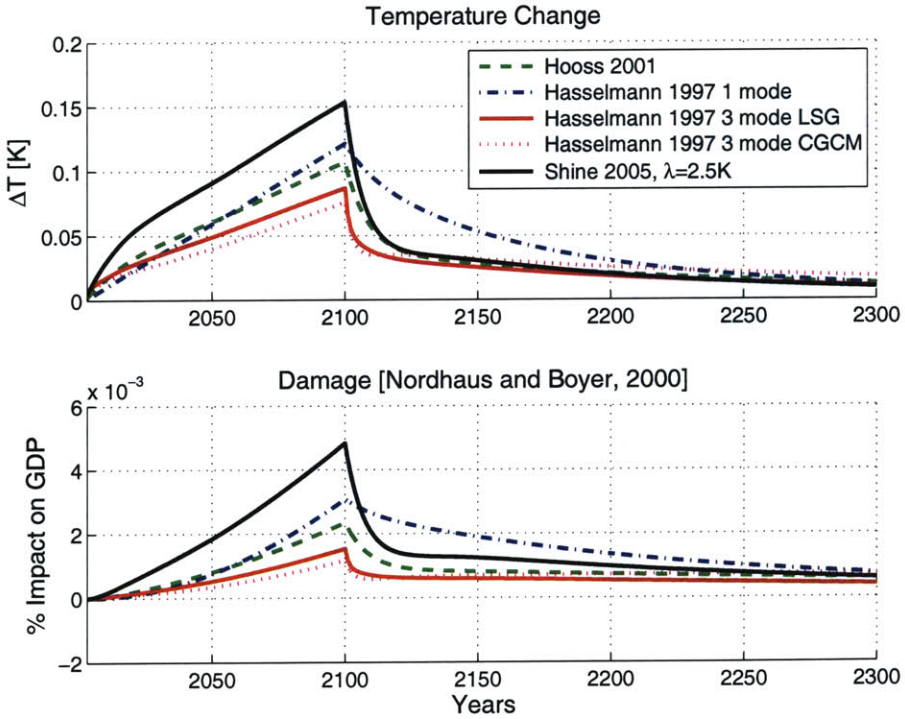

Figure 4-16: Impact of temperature response model

Case	Integrated Temperature Change [K·yr]		Integrated Damage Estimate [%GDP·yr]		NPV Estimate [2003US$ $\times 10^9$]	
	Sobol index	Total sensitivity	Sobol index	Total sensitivity	Sobol index	Total sensitivity
ΔT_{1900}^{ref}	-	-	0.1%	0.1%	0.2%	0.1%
RF_{2xCO_2}	0.9%	0.5%	1.6%	1.9%	1.4%	1.2%
RF^* short-lived	23.1%*	22.4%*	6.0%*	4.6%*	17.1%*	18.2%*
Short-lived efficacy	-1.1%	0.4%	-1.2%	0.1%	-1.1%	0.3%
Emission increment (fuelburn, CO_2)	2.3%	0.8%	1.3%	0.4%	1.8%	0.3%
Emission increment (NO_x)	1.8%	0.0%	2.0%	0.0%	1.8%	0.0%
e-folding time & $RFyr_{CH_4}$ & $RFyr_{short\ O_3}$ †	-0.6%	0.2%	-0.1%	0.1%	-0.5%	0.2%
e-folding time & $RFyr_{long\ O_3}$ & $RFyr_{short\ O_3}$ †	1.5%	0.0%	0.6%	0.0%	1.2%	0.0%
Climate sensitivity	74.1%*	77.3%*	92.7%*	94.4%*	78.3%*	83.3%*

† e-folding time, $RFyr_{CH_4}$ (or $RFyr_{long\ O_3}$), and $RFyr_{short\ O_3}$ were chosen as a group with a discrete distribution.

Table 4.11: Result of global sensitivity

Case	Temp. Change				Damage				Net Present Value			
	A1	A2	A3	A4	A1	A2	A3	A4	A1	A2	A3	A4
ΔT_{1900}^{ref}	-	-	-	-	7	5	8	5	7	4	9	7
RF_{2xCO_2}	5	3	7	4	3	3	4	3	3	3	5	3
RF^* short	2	2	2	2	2	2	2	2	2	2	2	2
Efficacy	4	8	6	5	5	6	6	5	4	7	7	4
Emission inc. (fuel-burn, CO_2)	3	7	3	3	4	7	5	4	5	9	3	4
Emission inc. (NO_x)	8	6	4	7	8	8	3	8	9	6	3	8
e-folding time & $RFyr_{CH_4}$ & $RFyr_{short\ O_3}$	6	4	8	6	6	4	8	5	6	5	8	6
e-folding time & $RFyr_{long\ O_3}$ & $RFyr_{short\ O_3}$	7	5	5	7	9	8	7	8	8	8	6	8
Climate sensitivity	1	1	1	1	1	1	1	1	1	1	1	1

where A1: MC regression, A2: VABO MC analysis, A3: Sobol' index, A4: Total sensitivity

Table 4.12: Rank comparison of uncertainty assessment results

4.6 Conclusion

All uncertainty assessment methods provide consistent results for significant input variables, climate sensitivity and short-lived RF. Uncertainty of climate sensitivity is most significant and uncertainty of short-lived RF is next. Table 4.12 shows the rank of four uncertainty assessment analysis methods. Overall rank is similar, but RF doubling CO_2 and short-lived efficacy are placed relatively in the lower rank and emission increment of NO_x is placed in the higher rank in the Sobol' index. This suggests the interactions related to RF for a doubling of CO_2 or efficacy are greater and the interaction related to the emission increment of NO_x is very small relative to other interactions. Also, the emission increment of fuel burn and CO_2 ranks lower in the VABO result compared to other results. The emission increment far from the base value, 0%, causes more variability because of nonlinearity.

Hybrid Monte-Carlo sensitivity analysis results show the choice of discount rate brings a completely different result overwhelming the impacts of scientific uncertainty. Also, the inconsistent contribution of scenario choices to each outputs suggests there are interactions between discount rate and a scenario choice although it is not presented numerically.

Chapter 5

Conclusions

5.1 Summary and Conclusions

This thesis introduced several uncertainty assessment methods and provided two example results applying these methods. Sensitivity analysis like NRSA or HMC analysis captures the response shift at a point. This type of sensitivity index is more suitable for deterministic models, but it can be applicable to probabilistic models by using probabilistic sampling like the HMC analysis. The HMC analysis is useful when assessing the assumptions and choices which cannot be represented as a distribution. The Monte Carlo regression analysis is an efficient method to rank the contributions of input variables because the analysis can be conducted with one simulation run regardless of the number of variables. As shown in the assessment of two APMT modules, the result of the MC regression analysis is also accurate for assessing the impacts of uncertainty if the response is close to a linear model. While the MC regression analysis assumes a response model, the VABO MC analysis does not require any assumption of output distributions. With a series of MC simulation runs that is the same as the number of input variables, the VABO MC analysis investigates the contribution of each variable individually. The results of the VABO MC analysis can be different according to the choice of baseline values if there is nonlinearity. Also, the impacts of the mean and variance shift in the VABO MC analysis are relative to the baseline values in contrast to the global sensitivity analysis which assesses the contribution of variables over their uncertainty range. The global sensitivity analysis requires the same number of MC simulations as the VABO MC analysis, but it requires a larger sampling size because the convergence rate of MC simulations is slower in the global sensitivity analysis than the

VABO MC analysis.

All uncertainty assessment methods provided the same ranking of significant variables in both examples. Two or three significant variables are clearly distinguished from other insignificant variables. In the price module, seat coefficients are the most significant parameters, and age is an insignificant factor between input variables of the regression model. In the climate module, all probabilistic analyses provided the same result that climate sensitivity and short-lived RF are most significant variables to contribute to the variability of all three outputs. However, the HMC analysis showed that discount rate is the most sensitive factor in the NPV estimation when considering assumptions and choices as well as probabilistic variables. Comparing the Sobol's index with the total sensitivity index shows that there are no significant interactions to change the ranking of significant variables in both modules. In the price module, the ranking of significant variables are almost similar even in a lower rank. In contrast, interaction effects between input variables are comparable to the main effect of lower ranking variables in the climate module, and as a result, the lower ranking of Sobol' indices does not agree with those of total sensitivity indices. Although all uncertainty assessment results are similar in the examples in this thesis, this result is not general, and must be determined for each individual module application as part of the assessment process.

For future work assessing these and other APMT modules the following process is suggested. First, analyze the model with the MC regression analysis. The MC regression analysis only requires one simulation run even with many input variables. To proceed to more complex analyses which require simulation runs as many as the number of input variables, sometimes it is required to screen insignificant variables to reduce computational efforts. The MC regression analysis provides relatively coarse results, but it is enough for screening variables. The insignificant variables can be fixed at their mean value rather than drawn as random samples. Next, proceed to one or more assessments of the VABO MC analysis, the global sensitivity analysis, or the HMC sensitivity analysis. If a researcher is interested in the uncertainty compared to the best estimation result, the VABO MC analysis is a more appropriate method. Global sensitivity analysis will provide better results if an assessment focuses on the uncertainty over the range not at points. Also, if there are many significant variables, the global sensitivity analysis will be a better choice to investigate the interaction effects. To present the sensitivity between nominal range limits or the impacts

of different assumptions and choices, the HMC sensitivity analysis is recommended.

5.2 Suggestion for Future Work

The following are recommended to improve the uncertainty assessment analysis:

- Global sensitivity analysis provides general uncertainty assessment with the same computation effort to VABO MC analysis in terms of the number of simulations. However, more sampling per simulation is required to reach reasonable convergence because the correlation between samples slows the convergence rate. One suggestion to improve the computational effort and convergence is applying a quasi-random sequences generation, called quasi-Monte Carlo, instead of a standard Monte Carlo simulation using pseudo-random numbers. Quasi Monte Carlo simulation generally gives better convergence and error than pseudo-random Monte Carlo simulation [32]. Applying quasi-Monte Carlo technique will be helpful for a complicate model requiring long running time like the climate module.

- The MC regression analysis result was very close to the total sensitivity result with the temperature change and the damage in the climate module, but the accuracy decreased in the NPV. The criterion such as R squared value for when the MC regression analysis is accurate enough should be suggested to use the MC regression result efficiently.

- The interaction effect can be investigated to compare the Sobol's index and the total sensitivity theoretically, but it is not applicable to compare the magnitude of two indices because of a different convergence rate. Therefore, it is recommended to assess the global sensitivity index for presenting the first order interaction directly if the interaction effect is important.

Also, it is recommended to improve the assessment of each module:

Price module The uncertainty inside the regression block should be investigated. In addition to assess the uncertainty in the performance or price of aircraft in the database with a probabilistic method, it is suggested to perform a sensitivity analysis with different database sources.

Climate module Interactions between input variables and assumptions or between assumptions should be investigated. One of approaches is Analysis of variance (ANOVA).

Appendix A

Summary of fitting result

A.1 Price Model

Fuel Cost Estimation:
$Fuel\ cost = -0.0000384 + 0.04018 \times CAROC$

Summary of Fit	
Rsquare	0.4307
Rsquare Adj	0.4241
Root Mean Square Error	0.000173
Mean of Response	0.000873
Observations	89

Table A.1: Fitting result of CAROC and fuel cost

Linear fit of ΔLC to aircraft price (per seat):
price per seat $= 0.2917 + 0.003539 \times \Delta LC$ *per seat*

Summary of Fit	
Rsquare	0.000385
Rsquare Adj	-0.01574
Root Mean Square Error	0.02350
Mean of Response	0.2916
Observations	64

Analysis of Variance

Source	DF	Sum of Squares	Mean Square	F ratio	Prob>F
Model	1	0.00001319	0.000013	0.0239	0.8776
Error	62	0.03423	0.000552		
C.Total	63	0.03424			

Table A.2: Fitting result of ΔLC and aircraft price (per seat) in the short-haul aircraft class

Linear fit of ΔLC to aircraft price (per seat):
price per seat $= 0.4069 - 0.06475 \times \Delta LC$ *per seat*

Summary of Fit	
Rsquare	0.1162
Rsquare Adj	0.09562
Root Mean Square Error	0.03148
Mean of Response	0.4075
Observations	45

Analysis of Variance

Source	DF	Sum of Squares	Mean Square	F ratio	Prob>F
Model	1	0.005601	0.005601	5.6522	0.0220
Error	43	0.04261	0.000991		
C.Total	44	0.04821			

Table A.3: Fitting result of ΔLC and aircraft price (per seat) in the long-haul aircraft class

Small seats class:

$(Lower - Avg)/Avg = -0.3290 + 0.002185 \times Avg.seats$

Summary of Fit	
Rsquare	0.8362
Rsquare Adj	0.7542
Root Mean Square Error	0.0196
Mean of Response	-0.0483
Observations	4

Table A.4: Fitting result of (Lower - Average)/Average

Large seats class:

$(Lower - Avg)/Avg = 0 + 0 \times Avg.seats$

Summary of Fit	
Rsquare	.
Rsquare Adj	.
Root Mean Square Error	0
Mean of Response	0
Observations	9

Table A.5: Fitting result of (Lower - Average)/Average

Small seats class:

$(Upper - Avg)/Avg = -3.2108 + 0.6792 \times \log Avg.seats$

Summary of Fit	
Rsquare	0.9578
Rsquare Adj	0.9367
Root Mean Square Error	0.0221
Mean of Response	0.0831
Observations	4

Table A.6: Fitting result of (Upper - Average)/Average

Large seats class:

$(Upper - Avg)/Avg = -0.85 + 0.2095 \times \log Avg.seats$

Summary of Fit	
Rsquare	.
Rsquare Adj	.
Root Mean Square Error	0.1799
Mean of Response	0.3049
Observations	9

Table A.7: Fitting result of (Upper - Average)/Average

Short-haul aircraft class

Summary of Fit	
Rsquare	0.9980
Rsquare Adj	0.9980
Root Mean Square Error	0.3411
Mean of Response	50.3430
Observations	10000

Table A.8: Fitting result of first order regression with MC simulation in short-haul aircraft

Long-haul aircraft class

Summary of Fit	
Rsquare	0.9915
Rsquare Adj	0.9915
Root Mean Square Error	1.2271
Mean of Response	98.8548
Observations	10000

Table A.9: Fitting result of first order regression with MC simulation in long-haul aircraft

A.2 Climate Model

Temperature Change

Summary of Fit	
Rsquare	0.9781
Rsquare Adj	0.9780
Root Mean Square Error	1.0822
Mean of Response	20.5804
Observations	3000

Table A.10: Fitting result of first order regression with MC simulation in the temperature change

Damage

Summary of Fit	
Rsquare	0.9646
Rsquare Adj	0.9644
Root Mean Square Error	0.1071
Mean of Response	0.9800
Observations	3000

Table A.11: Fitting result of first order regression with MC simulation in the damage

Net Present Value

Summary of Fit	
Rsquare	0.9451
Rsquare Adj	0.9448
Root Mean Square Error	1104.4122
Mean of Response	8021.0367
Observations	3000

Table A.12: Fitting result of first order regression with MC simulation in the NPV

Appendix B

Reference Data

B.1 Price Model

	Dollar conversion factor (year $i \rightarrow 2004$)	Fuel price of year i in 2004\$ (\$/gallon)
1988	0.626	0.855
1990	0.692	1.132
1992	0.743	0.857
1994	0.785	0.711
1996	0.831	0.800
1998	0.863	0.594
2000	0.912	0.884
2002	0.952	0.750
2004	1.000	1.146

Fuel price source: Energy Information Administration (EIA)

Table B.1: Dollar conversion factor and historical fuel price used in the CAROC and price conversion

B.2 Climate Model

	CO_2 Background Emission (Tt(C))			World GDP Preojection (US$B)		
	IS92a	IS92c	IS92e	IS92a	IS92c	IS92e
1985	6.5163	6.5173	6.5163	16984.9	16984.9	16984.9
1990	7.4050	7.4060	7.4050	20107.0	20107.0	20107.0
1995	7.9312	7.2298	8.1589	23136.4	21292.2	24293.1
2000	8.4432	7.4646	9.0995	26737.6	23925.4	29169.1
2005	9.1585	7.7534	10.1718	31260.9	27239.0	35829.8
2010	9.8882	8.0516	11.3968	36484.3	30717.7	43421.4
2015	10.6424	8.3092	12.6257	41737.3	33542.7	51245.9
2020	11.3764	8.4939	13.7417	47735.0	36379.4	59956.5
2025	12.2289	8.7880	15.0834	54657.8	39190.6	69595.0
2050	14.5242	7.5103	20.1043	92405.1	48915.9	138392.2
2075	16.3147	5.5803	26.9569	152783.7	57445.0	270557.1
2100	20.2771	4.6148	35.8443	243147.0	64774.6	520529.2

Data source: The IPCC Data Distribution Centre
(http://sedac.ciesin.org/ddc/is92/index.html)

Table B.2: IS92 scenarios data

	Aviation Emission Scenario								
	CO_2 (Tg(C))			NO_x (Tg(NO_x))			Fuelburn (Tg(fuel))		
	Fa1	Fc1	Fe1	Fa1	Fc1	Fe1	Fa1	Fc1	Fe1
2003	151.80	151.80	151.80	2.49	2.49	2.49	176.43	176.43	176.43
2015	217.35	217.35	217.35	4.12	4.12	4.12	252.73	252.73	252.73
2050	340.70	192.70	533.20	6.10	3.50	9.60	396.10	224.00	620.00
2100	560.45	316.99	877.11	10.03	5.76	15.79	651.58	368.48	1019.9

2003: SAGE inventories, 2015: NASA estimation, 2050: FESG scenarios, 2100: 1% growth after 2050

Table B.3: Aviation scenarios data

Bibliography

[1] Federal Aviation Administration. Sage: Validation assessment, model assumptions and uncertainties. Technical Report FAA-EE-2005-03, Federal Aviation Administration, Whshington D.C., 2005.

[2] Federal Aviation Administration. Sage: Version 1.5 technical manual. Technical Report FAA-EE-2005-01, Federal Aviation Administration, Whshington D.C., 2005.

[3] F.M.F. ASME, H. Zhang, A. Bockstedte, GC Foliente, and P. Paevere. Parameter Analysis of the Differential Model of Hysteresis. *Journal of Applied Mechanics*, 71:342, 2004.

[4] D.G. Cacuci, M. Ionescu-Bujor, and I.M. Navon. *Sensitivity and Uncertainty Analysis.* CRC Press, 2003.

[5] CAEP/4-FESG. Report 4. report of the forecasting and economic anaylsis sub-group (fesg): Long-range scenarios. Technical report, International Civil Aviation Organization Committee on Aviation Environmental Protection Steering Group Meeting, Canberra, Australia, January 1998.

[6] U. Cubasch, K. Hasselmann, H. Höck, E. Maier-Reimer, U. Mikolajewicz, B.D. Santer, and R. Sausen. Time-dependent greenhouse warming computations with a coupled ocean-atmosphere model. *Climate Dynamics*, 8(2):55–69, 1992.

[7] RI Cukier, CM Fortuin, KE Shuler, AG Petschek, and JH Schaibly. Study of the sensitivity of coupled reaction systems to uncertainties in rate coefficients. I Theory. *The Journal of Chemical Physics*, 59:3873–3879, 1973.

[8] RI Cukier, JH Schaibly, and KE Shuler. Study of the sensitivity of coupled reaction systems to uncertainties in rate coefficients. III Analysis of the approximations. *The Journal of Chemical Physics*, 63:1140–1149, 1978.

[9] GJ Daniell, AJG Hey, and JE Mandula. Error analysis for correlated Monte Carlo data. *Physical Review D*, 30(10):2230–2232, 1984.

[10] B. Efron and R. Tibshirani. Bootstrap Methods for Standard Errors, Confidence Intervals, and Other Measures of Statistical Accuracy. *Statistical Science*, 1(1):54–75, 1986.

[11] Partnership for AiR Transportation Noise and Emissions Reduction (PARTNER). Architecture study for the aviation environmental portfolio management tool (apmt). Technical report, An FAA/NASA/Transport Canada-sponsored Center of Excellence, 2006.

[12] H.C. Frey and S.R. Patil. Identification and review of sensitivity analysis methods. *Risk Analysis*, 22(3):553–578, 2002.

[13] J.S. Fuglestvedt, T.K. Berntsen, O. Godal, R. Sausen, K.P. Shine, and T. Skodvin. Metrics of Climate Change: Assessing Radiative Forcing and Emission Indices. *Climatic Change*, 58(3):267–331, 2003.

[14] A.A. Giunta, S.F. Wojtkiewicz Jr, and M.S. Eldred. Overview of Modern Design of Experiments Methods for Computational Simulations. *AIAA Paper*, 649:2003, 2003.

[15] J. Guo, C.J. Hepburn, R.S.J. Tol, and D. Anthoff. Discounting and the social cost of carbon: a closer look at uncertainty. *Environmental Science and Policy*, 9(3):205–216, 2006.

[16] J. Hansen, M. Sato, R. Ruedy, L. Nazarenko, A. Lacis, GA Schmidt, G. Russell, I. Aleinov, M. Bauer, S. Bauer, et al. Efficacy of climate forcings. *J. Geophys. Res*, 110, 2005.

[17] K. Hasselmann, S. Hasselmann, R. Giering, V. Ocana, and HV Storch. Sensitivity Study of Optimal CO 2 Emission Paths Using a Simplified Structural Integrated Assessment Model (SIAM). *Climatic Change*, 37(2):345–386, 1997.

[18] K. Hasselmann, R. Sausen, E. Maier-Reimer, and R. Voss. On the cold start problem in transient simulations with coupled atmosphere-ocean models. *Climate Dynamics*, 9(2):53–61, 1993.

[19] JC HELTON. Uncertainty and sensitivity analysis techniques for use in performance assessment for radioactive waste disposal. *Reliability engineering & systems safety*, 42(2-3):327–367, 1993.

[20] Great Britin H.M.Treaury. *Green Book: Appraisal and Evaluation in Central Government.* TSO, London, 2003.

[21] T. Homma and A. Saltelli. Importance measures in global sensitivity analysis of nonlinear models. *Reliability Engineering and System Safety*, 52(1):1–17, 1996.

[22] G. Hooss, R. Voss, K. Hasselmann, E. Maier-Reimer, and F. Joos. A nonlinear impulse response model of the coupled carbon cycle-climate system (NICCS). *Climate Dynamics*, 18(3):189–202, 2001.

[23] M. Hulme and TR Carter. Representing uncertainty in climate change scenarios and impact studies. *Representing Uncertainty in Climate Change Scenarios and Impact Studies. Proceedings of the ECLAT-2 Helsinki Workshop, 14–16 April, 1999*, pages 11–37, 1999.

[24] Third Assessment Report Intergovernmental Panel on Climate Change (IPCC) Working Group I. Climate change 2001: The scientific basis. Technical report, IPCC, 2001.

[25] F. Joos, I.C. Prentice, S. Sitch, R. Meyer, G. Hooss, G.K. Plattner, S. Gerber, and K. Hasselmann. Global warming feedbacks on terrestrial carbon uptake under the Intergovernmental Panel on Climate Change (IPCC) emission scenarios. *Global Biogeochemical Cycles*, 15(4):891–907, 2001.

[26] V. Kreinovich, J. Beck, C. Ferregut, A. Sanchez, GR Keller, M. Averill, and SA Starks. Monte-carlo-type techniques for processing interval uncertainty, and their engineering applications. *Proc. NSF workshop on reliable engineering computing*, 2004.

[27] M.H. Kutner, Nachtsheim C.J., Neter J., and Li W. *Applied Linear Statistical Models.* McGraw-Hill/Irwin, 2004.

[28] Ian A. Waitz Brian Y. Kim Gregg G. Fleming Lourdes Maurice Curtis A. Holsclaw Lee, Joosung J. Lee. System for assessing aviation's global emissions (sage): Uncertainty assessment. Technical report, In preparation, 2006.

[29] J. Markish. *Valuation Techniques for Commercial Aircraft Program Design.* PhD thesis, Massachusetts Institute of Technology, Dept. of Aeronautics and Astronautics, 2002.

[30] D.N. Mavris and O. Bandte. Economic Uncertainty Assessment Using a Combined Design of Experiments/Monte Carlo Simulation Approach with Application to an HSCT. *17th ISPA Conference, San Diego, CA, May*, 1995.

[31] The Airline Monitor. www.airlinemonitor.com, 2005.

[32] W.J. Moroko and R.E. Caisch. Quasi-Monte Carlo integration. *J. Comp. Phys*, 122:218–230, 1995.

[33] M. New and M. Hulme. Representing uncertainty in climate change scenarios: a Monte-Carlo approach. *Integrated Assessment*, 1(3):203–213, 2000.

[34] R.G. Newell and W.A. Pizer. Discounting the Distant Future: How Much Do Uncertain Rates Increase Valuations? *Journal of Environmental Economics and Management*, 46(1):52–71, 2003.

[35] R.G. Newell and W.A. Pizer. Uncertain discount rates in climate policy analysis. *Energy Policy*, 32(4):519–529, 2004.

[36] W.D. Nordhaus and J. Boyer. *Warming the World: Economic Models of Global Warming.* Mit Pr, 2000.

[37] GK Plattner, F. Joos, TF Stocker, and O. Marchal. Feedback mechanisms and sensitivities of ocean carbon uptake under global warming. *Tellus B*, 53(5):564, 2001.

[38] A. Saltelli and R. Bolado. An alternative way to compute Fourier amplitude sensitivity test (FAST). *Computational Statistics and Data Analysis*, 26(4):445–460, 1998.

[39] R. Sausen, I. Isaksen, V. Grewe, D. Hauglustaine, D.S. Lee, G. Myhre, M.O. Köhler, G. Pitari, U. Schumann, F. Stordal, et al. Aviation radiative forcing in 2000: An update on IPCC (1999). *Meteorologische Zeitschrift*, 14(4):555–561, 2005.

[40] R. Sausen and U. Schumann. Estimates of the Climate Response to Aircraft CO 2 and NO x Emissions Scenarios. *Climatic Change*, 44(1):27–58, 2000.

[41] J.H. Schaibly and K.E. Shuler. Study of the sensitivity of coupled reaction systems to uncertainties in rate coefficients. II Applications. *The Journal of Chemical Physics*, 59:3879–3888, 1973.

[42] K.P. Shine, J.S. Fuglestvedt, K. Hailemariam, and N. Stuber. Alternatives to the Global Warming Potential for Comparing Climate Impacts of Emissions of Greenhouse Gases. *Climatic Change*, 68(3):281–302, 2005.

[43] IM Sobol. Sensitivity estimates for nonlinear mathematical models. *Matematicheskoe Modelirovanie*, 2:112–118, 1990.

[44] IM Sobol. Sensitivity estimates for nonlinear mathematical models. *Mathematical Modeling and Computational Experiment*, 1(4):407–414, 1993.

[45] IM Sobolá. Global sensitivity indices for nonlinear mathematical models and their Monte Carlo estimates. *Mathematics and Computers in Simulation*, 55(1-3):271–280, 2001.

[46] D.S. Stevenson, R.M. Doherty, M.G. Sanderson, W.J. Collins, C.E. Johnson, and R.G. Derwent. Radiative forcing from aircraft NO x emissions: mechanisms and seasonal dependence. *J. Geophys. Res*, 109, 2004.

[47] R.S.J. Tol. The marginal damage costs of carbon dioxide emissions: an assessment of the uncertainties. *Energy Policy*, 33(16):2064–2074, 2005.

[48] M.L. Weitzman. Gamma Discounting. *The American Economic Review*, 91(1):260–271, 2001.